Lithos 336–337 (2019) 151–168

Contents lists available at ScienceDirect

Lithos

journal homepage: www.elsevier.com/locate/lithos

The role of subducted sediments in the formation of intermediate mantle-derived magmas from the Northern Colombian Andes

Carlos Errázuriz-Henao [a,b], Arturo Gómez-Tuena [c,*], Jose Duque-Trujillo [b], Marion Weber [a]

[a] Departamento de Geociencias y Medio Ambiente, Facultad de Minas, Universidad Nacional de Colombia, Carrera 80 No. 65-223, Medellín, Colombia
[b] Departamento de Ciencias de la Tierra, Universidad EAFIT, Carrera 49 No. 7 Sur-50, Medellín, Colombia
[c] Centro de Geociencias, Universidad Nacional Autónoma de México, Querétaro 76230, Mexico

ARTICLE INFO

Article history:
Received 9 January 2019
Accepted 4 April 2019
Available online 9 April 2019

Keywords:
Subduction
Andes
Andesites
Carbonate subduction

ABSTRACT

Unraveling the sources and processes that produce intermediate continental arc volcanoes is still a challenge for geoscientists. To address this problem, here we use comprehensive geochemical and isotopic data from Nevado del Santa Isabel and Cerro Machín volcanoes in the North Volcanic Province of Colombia, and from oceanic sediments sampled outboard the Colombian continental margin. Volcanoes along this province have been influenced by the subduction of a compositionally contrasting sedimentary column constituted by a carbonate-rich pelagic layer overlain by a clay-and-apatite-rich hemipelagic unit. The studied volcanoes exhibit the high Mg# (~60) and calc-alkaline affinities that are typical of continental arcs but display unusually high and contrasting Th(U)/La, Nb/Ta and Dy/Yb ratios and isotopic compositions. We argue that the geochemical variations within and among these volcanoes are not controlled by differentiation or crustal contamination of a parental basaltic magma but formed by melting of different kinds of subducted sedimentary materials detached from the slab as buoyantly rising diapirs at various depths. This model accounts for the reworking of refractory carbonates into arc magmatism and suggests that the geochemical diversity of the North Volcanic Province is mainly controlled by the nature of the subduction inputs and their exhumation pathways within the mantle wedge.

1. Introduction

Andesite petrogenesis and their relation to convergent margins have long been a puzzling problem for Earth Scientists (Gill, 1981; Gómez-Tuena et al., 2014a; Taylor, 1967). Most researchers concur that global intermediate arc magmas represent mixtures between juvenile mantle-like components and pre-existent crust-like materials (Gill, 1981; Taylor, 1967). Nonetheless, current petrogenetic models fail to agree on whether this hybridization process occurs through assimilation or mingling in the overriding crust (Annen et al., 2006; Bezard et al., 2014; Hildreth and Moorbath, 1988) or in the mantle wedge via the incorporation of crustal and sedimentary components into the subduction channel (Behn et al., 2011; Gómez-Tuena et al., 2014b; Nielsen and Marschall, 2017; Straub et al., 2011). This is a complex problem because most of the crustal materials introduced into the mantle wedge, such as sediments or ablated forearc debris, display very similar compositional characteristics to the overriding continental crust (Clift et al., 2009; Parolari et al., 2018; Plank and Langmuir, 1998) and therefore the origin and evolution of andesites can be obscured by a variety of processes that combine similar components. Despite these limitations, there are a few convergent margins where the subducted trench sediments differ from the Global Subducted Sediment (GLOSS), which arguably carries the typical characteristics of the upper continental crust (Plank, 2013; Plank and Langmuir, 1998). This is the case of the Colombian Andean margin, where carbonate-rich pelagic and hemipelagic sediments are not only being introduced into the mantle wedge in enormous quantities, but also transferred back to the atmosphere by degassing from arc volcanoes of the Northern Volcanic Zone of the Andes (Aiuppa et al., 2017). Volcanoes in this region are thus in a privileged position to investigate the influence of subducted sedimentary carbonate in the source of a thick-crusted continental arc.

The North Volcanic Province of Colombia (NVP) is mostly constituted by high-Mg# calc-alkaline intermediate volcanic rocks with characteristics that are typical of continental arcs (Kelemen et al., 2003). And yet two of the most studied volcanoes in the region, Nevado del Ruiz and Cerro Machín, display contrasting trace element and isotopic characteristics that have been attributed to contamination with a pre-existent continental crust (Laeger et al., 2013; Vatin-Pérignon et al., 1988). Since both volcanoes have been emplaced on top of the same local basement and share an almost identical crustal architecture, the possibility exists that their sources may have been influenced by different subduction components. To test this hypothesis, in this contribution we report whole-rock geochemical data and Pb, Sr, Nd and Hf isotopic

* Corresponding author.
E-mail address: tuena@geociencias.unam.mx (A. Gómez-Tuena).

https://doi.org/10.1016/j.lithos.2019.04.007
0024-4937/

compositions of volcanic rocks from Nevado del Santa Isabel (NSI) and Cerro Machín (CMV) volcanoes, located in the center and south of the NVP, respectively. To further constrain the subduction inputs, we also present new geochemical and isotopic data from sedimentary sequences sampled outboard the North Andean Colombian margin. This information, along with geophysical and geological data of the Northern Andes, is used to evaluate the sources and processes involved in magma genesis along magmatic arcs, in light of one of the least sampled and studied volcanic areas on Earth.

2. Geologic setting

The North Volcanic Province (NVP) of the Colombian Central Cordillera is a ~65 km long Quaternary volcanic chain that represents the northernmost expression of polygenetic volcanic activity in the Andes (Fig. 1a). The currently active volcanoes are related to subduction of the Nazca Plate beneath the South American Plate (Gutscher et al., 1999). The province is essentially constituted by andesitic-dacitic products distributed in a N-S alignment of polygenetic volcanoes named from north to south as: Cerro Bravo, Nevado del Ruiz, Nevado del Santa Isabel, Paramillo de Santa Rosa, Paramillo del Quindío, Nevado del Tolima and Cerro Machín (Fig. 1b). At the trench, the ca. 12 Ma Nazca plate converges at a rate of ~60 mm/year (Lonsdale, 2005; Syracuse et al., 2010; Syracuse et al., 2016) with a subduction angle that varies from 15° to 25° along strike (Gutscher et al., 1999). North of the NVP, seismic reflectors of the Nazca Plate are shifted towards the Eastern Cordillera, forming a flat slab section where polygenetic volcanic activity is absent (Chiarabba et al., 2016) (Fig. 1a). To the south, the Nazca Plate plunges with a nearly vertical geometry and the volcanic activity also ceases until ~2°N as the slab dip becomes gentler (Syracuse et al., 2016). Along the NVP, the subduction dip-direction shifts to the SE, forming a southward gradual increase in arc front slab-depths from 120 km at the northernmost volcano (Cerro Bravo) to 160 km below the southernmost volcano (Cerro Machín) (Hayes et al., 2012) (Fig. 1a).

Volcanoes of the NVP are emplaced on top of a ~42–52 km thick continental crust that becomes slightly thicker southwards (up to 52) (Poveda et al., 2015; Poveda et al., 2018; Yarce et al., 2014), following a tectonic lineament defined by the right-lateral Palestina fault system (Borrero et al., 2009). Magmas of the NVP intrude and rest on top of Paleozoic metapelites metamorphosed at green-schist and amphibolite facies of the Cajamarca Complex, which comprises the metamorphic core of the Colombian Central Cordillera (Villagómez et al., 2011). The lower crustal lithological assemblages in the Andean region are assumed to be similar to a set of high-pressure (10–14 kbar) pyroxenites, granulites and hornblendites found as xenoliths in the South Volcanic Province (SVP) of Colombia (Weber, 1998), which have been recently dated at <5 Ma by Lu-Hf in garnets (Bloch et al., 2017). The origin of these xenoliths is not yet fully understood; they have been related to subduction accretion due to oceanic-arc collision (Weber et al., 2002) or to a recent crustal foundering event of a gravitationally unstable lower crust (Bloch et al., 2017). Regardless, these xenoliths are important because they have been used as crustal contaminants in petrogenetic studies of Quaternary volcanism in the SVP (Marín-Cerón et al., 2010).

The sedimentary packages sampled offshore the Colombian trench (Fig. 1) are characterized by two lithological and geochemically contrasting lithologies: an Upper Miocene pelagic biogenic carbonate unit made of limestone and chalk, which is characterized by high $CaCO_3$ and lower organic carbon contents (Fig. 2a), and a Plio-Pleistocene clay-bearing nannofossil-rich hemipelagic ooze unit with higher organic carbon (Fig. 2a) (Beiersdorf and Natland, 1983). The upsection decrease in $CaCO_3$ contents outlines the so-called “carbonate crash”, a palaeoceanographic event across the western Caribbean and Eastern Pacific basins attributed to changes in deep water circulation due to the closure of the Central American Seaway in the middle-late Miocene (Jiang et al., 2007; Lyle et al., 1995).

3. Samples

The volcanic rocks studied here were collected at Nevado del Santa Isabel (NSI), a 10 km long succession of andesitic lava flows and domes with eruptive ages ranging from 0.76-0.64 Ma to 5-3.5 ka (Thouret et al., 1990). Rocks from NSI are compositionally similar to nearby Nevado del Ruiz stratovolcano (Martínez et al., 2014). In order

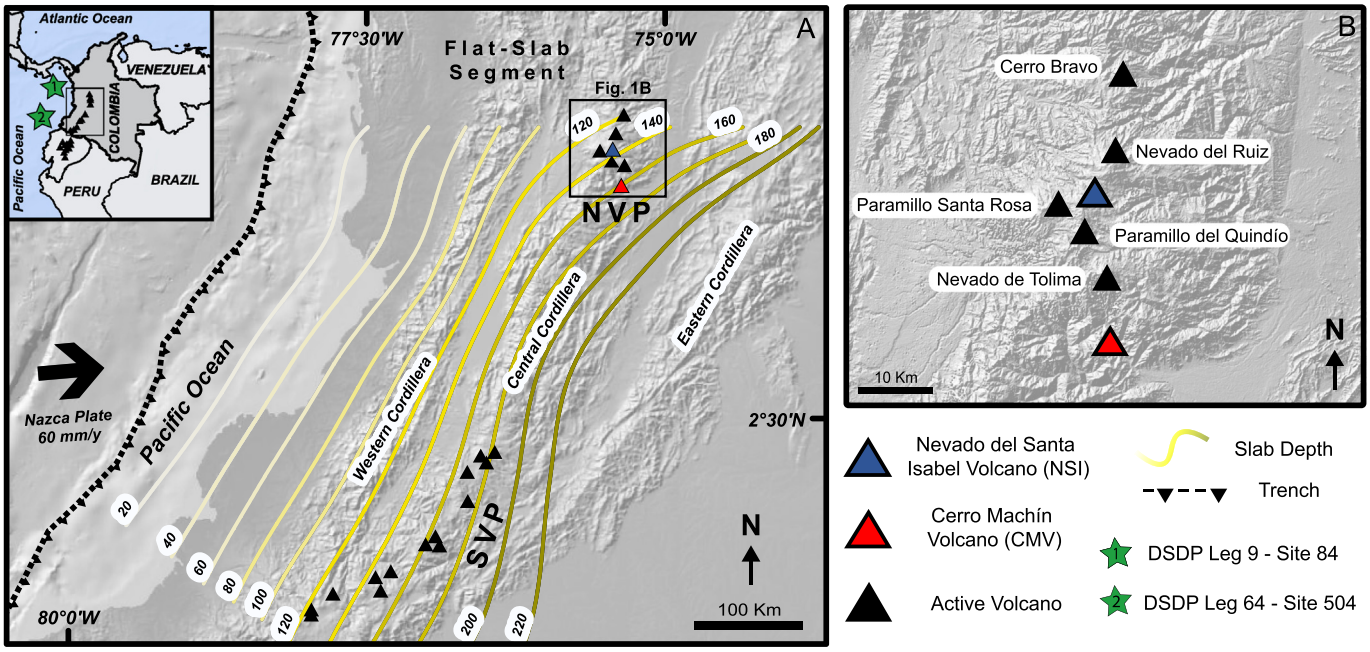

Fig. 1. Tectonic map of the Northern Volcanic Zone of Colombia and the studied area. (A) North Volcanic Province (NVP) and South Volcanic Province (SVP). Gray-scale lines represent the slab geometry of the subducted Nazca Plate (Hayes et al., 2012). Triangles represent active volcanoes. DSDP sites located offshore Ecuador/Colombia (Site 504) and Panama/Colombia (Site 84) (inset). (B) Main active volcanoes of the NVP.

to further understand the geochemical variations along strike, we also analyzed newly collected samples from the southernmost composite volcano, Cerro Machín (CMV), a 0.5–0.09 ka intra-crateric dome structure with associated plinian deposits located 40 km to the south of NSI (Laeger et al., 2013; Piedrahita et al., 2018) and from an adjacent small dome structure (sample MOR-01), which is considered here to be genetically related to CMV based on its composition.

About 300 m of sediments were sampled by drill cores of the Deep Sea Drilling Program (DSDP) Expedition 59 (Sites 504–505) offshore Colombia/Ecuador, and by DSDP Expedition 9 (Site 84) offshore Panama/Colombia (Fig. 1a, inset). The sedimentary columns were previously analyzed geochemically for a selected number of elements (Beiersdorf and Natland, 1983). However, to better characterize the geochemical compositions of the subducted sedimentary sequences, we re-analyzed representative core samples along both sections (Fig. 2, Table 1). Samples from the upper carbonate-poor units on both DSDP Sites are characterized by their higher U, Th and Rb contents, which translate to higher U/La, Th/La and Rb/La ratios (Fig. 2a). In contrast, the lower carbonate-rich units have much higher Sr contents and an overall depletion in most trace elements when compared to the upper units (Fig. 2b). Based on our new analyses of these representative samples, we calculated the average compositions of the hemipelagic upper units and the carbonate lower units (Table 1). These bulk compositions were then used to evaluate their potential role in arc magmatism along the NVP.

The Colombian sediments are compositionally similar to the Central American trench sediments sampled at ODP Site 895 (Plank et al., 2002; Vervoort et al., 2011), especially in their U, Th and Rb enrichments to the top of the sequences (Fig. 2). Yet, the Colombian trench sediments show a clear enrichment in organic matter in both the upper and lower units, and also higher $CaCO_3$ contents in the upper unit when compared to those from Central America. Among the global spectrum of subducted sediments, the Colombian sedimentary column displays one of the highest bulk carbonate contents and thus anomalously high CaO concentrations (up to 45 wt%) (Plank, 2013). The Colombian trench sediments thus show trace element patterns that differ significantly from the composition of the GLOSS (Plank, 2013). They are more depleted in REE, HFSE and incompatible elements as Cs, Rb, Th and Pb, but show substantial enrichments in Sr, Ba and U contents (Fig. 2b).

4. Analytical methods

Samples from NSI and CMV where initially crushed in a hydraulic press and then sieved to select <5 mm chips. Fresh hand-picked chips where then ultrasonically washed in deionized water, dried and powdered in an alumina mill and shatter box for major and trace element chemical preparations. Hand-picked rock chips of 2–3 mm in size were leached and dissolved in acids for isotopic analysis. Sedimentary core samples were first dried and then powdered by hand on an alumina mortar before digestion for trace element and isotopic analysis without leaching.

For major and trace element analysis, about 50 mg of rock powders were digested using high pressure Parr bombs to adequately dissolve resistant mineral species, followed by open vessel acid dissolution procedures described in Mori et al. (2007). The elemental concentrations were determined by Inductively Coupled Plasma Mass Spectrometry (ICP-MS) using a Thermo iCap-Qc at Laboratorio de Estudios Isotópicos (LEI) at the Centro de Geociencias (CGeo), UNAM (Table 1: DSDP sediments; Appendix A: volcanic rocks). SiO_2 concentrations were not directly analyzed and the reported values are estimated by differences from the total on an anhydrous basis. Reproducibility and accuracy of major and trace element data at CGeo are given by the average concentrations and standard deviations of multiple digestions of different rock standards (AGV-2, BHVO-2, BCR-2, JB-2 and internal standard PS-99-25; Appendix C), and has been reported in several previous publications (Gómez-Tuena et al., 2011; Mori et al., 2007).

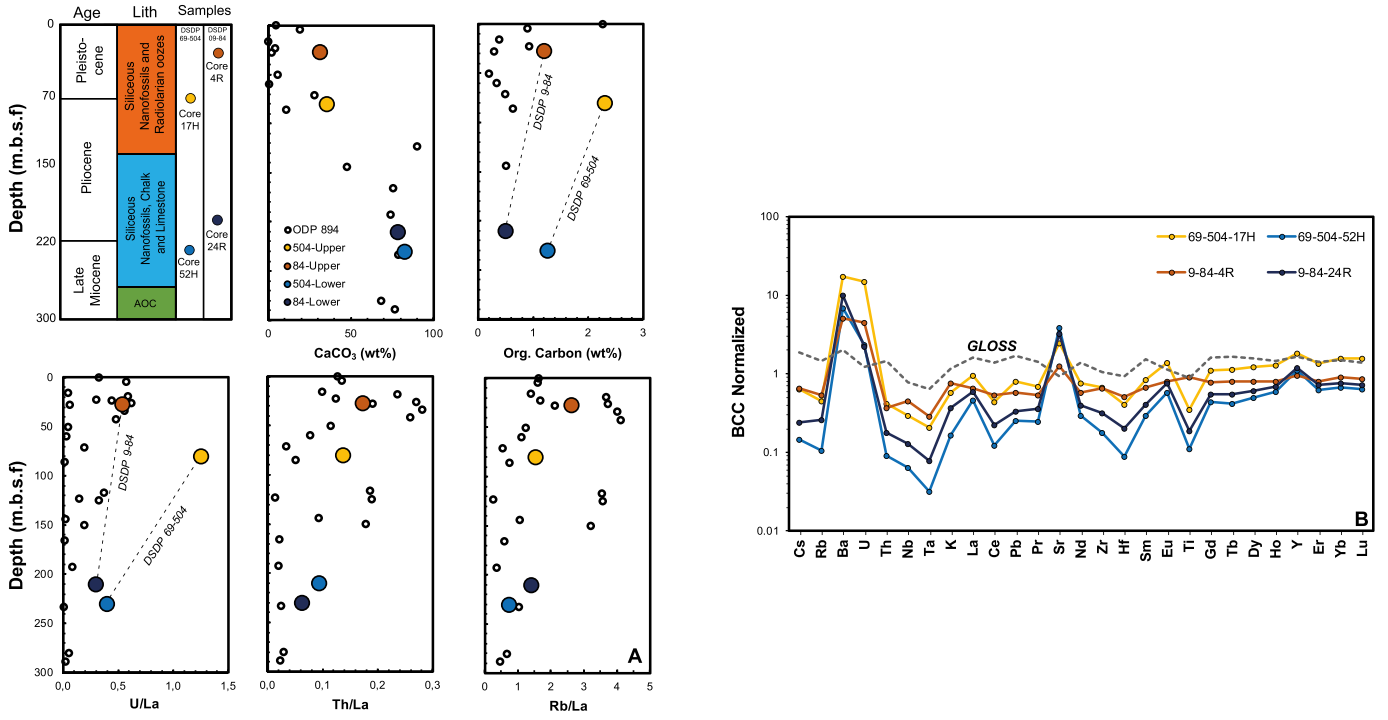

Fig. 2. (A) Schematic sedimentary column for DSDP sites 504 and 84 outboard the Colombian margin, locations of selected key samples and their geochemical variability along the sequence. Selection of samples based on lithological units along the sedimentary column (Beiersdorf and Natland, 1983; Beiersdorf and Rösch, 1983). Also shown for comparison are the Central American trench sediments which display a similar stratigraphic distribution along the sequence (Plank et al., 2002; Vervoort et al., 2011). Both Colombian and Central American sediments display a reduction in $CaCO_3$ concentrations and an enrichment in organic content and incompatible trace elemental abundances to the top of the column. (B) Multi-element plot normalized to the Bulk Continental Crust (BCC) from Rudnick (1995). We also show the average Global Subducting Sediment (GLOSS II) from Plank (2013) for comparison. Overall, trench sediments from Colombia are compositionally different to GLOSS II, which shows higher LILE, HFSE and REE concentrations but lower Ba, U and Sr contents.

Table 1
Major, trace element and isotopic compositions from the DSDP sites offshore Colombia and calculated Bulk Upper and Lower Units.

DSDP (site-hole)	69–504	69–504	9–84	9–84	Bulk upper hemipelagic unit	Bulk lower carbonate unit
Sample (core-section)	17H-3	52H-1	4R-4	24R-3		
Core depth (m.b.s.f)	80	230	27	210		
Description	Siliceous-nannofossil ooze	Siliceous-nannofossil chalk	Radiolarian-nannofossil ooze	Radiolarian-nannofossil chalk		
Depth in core (min) [cm]	65	60	10	120		
Depth in core (max) [cm]	70	65	15	125		
Major elements (wt%)[a]						
TiO_2	0.2	0.1	0.6	0.1	0.4	0.1
Al_2O_3	6.54	1.84	12.1	3.18	9.33	2.51
$Fe_2O_3^{tot}$	4.0	1.7	6.5	3.3	5.3	2.5
MnO	0.29	0.16	0.34	0.098	0.32	0.13
MgO	1.7	0.89	2.9	1.6	2.3	1.3
CaO	14	46	9.6	31	11.6	38.7
Na_2O	4.3	1.6	4.7	2.3	4.5	2.0
K_2O	1.1	0.31	1.4	0.69	1.3	0.5
P_2O_5	0.16	0.14	0.14	0.12	0.15	0.13
$CaCO_3$[b]	35	82	31	78	33	80
Org. Carbon[b]	2.3	1.3	1.2	0.50	1.8	0.88
Trace elements (ppm)						
Sc	14.3	2.97	20.3	4.38	17.3	3.67
V	257.7	51.4	191.2	66.3	224.4	58.9
Cr	50.5	12.7	74.3	20.8	62.4	16.7
Co	25.9	7.49	23.3	11.3	24.6	9.39
Ni	331	73.3	141	74.7	236	74.0
Cu	277	74	120	75	199	74
Zn	402	111	227	112	315	111
Ga	12.7	4.07	13.9	5.17	13.3	4.62
Li	23.8	10.9	76.9	17.2	50.3	14.0
Be	1.1	0.42	0.93	0.53	1.0	0.48
Rb	26	6.1	31	15	28	11
Sr	792	1246	406	1058	599	1152
Y	36.9	22.2	19.2	24.1	28.1	23.2
Zr	82.1	21.7	79.8	39.4	81.0	30.6
Nb	3.50	0.777	5.41	1.55	4.45	1.16
Mo	86.4	2.05	6.60	9.97	46.5	6.0
Sn	0.65	0.25	0.77	0.33	0.71	0.29
Sb	16	1.6	7.6	1.4	12	1.5
Cs	1.65	0.385	1.72	0.625	1.68	0.505
Ba	6774	2652	2003	3892	4388	3272
La	17.1	8.37	11.9	10.7	14.5	9.53
Ce	18.4	5.20	22.6	9.44	20.5	7.32
Pr	3.41	1.25	2.71	1.79	3.06	1.52
Nd	15.1	5.96	11.7	8.01	13.4	6.99
Sm	3.31	1.14	2.65	1.59	2.98	1.37
Eu	1.67	0.697	0.964	0.921	1.31	0.809
Gd	3.96	1.59	2.81	2.00	3.39	1.80
Tb	0.630	0.237	0.451	0.305	0.540	0.271
Dy	4.24	1.74	2.83	2.13	3.54	1.94
Ho	0.978	0.452	0.613	0.528	0.796	0.490
Er	2.96	1.36	1.76	1.57	2.36	1.47
Yb	3.13	1.34	1.82	1.54	2.47	1.44
Lu	0.523	0.213	0.285	0.242	0.404	0.228
Hf	1.51	0.330	1.88	0.744	1.69	0.537
Ta	0.227	0.035	0.319	0.087	0.273	0.061
W	0.520	0.163	0.739	0.247	0.630	0.205
Tl	3.16	0.445	1.47	0.388	2.31	0.417
Pb	8.16	3.23	7.27	4.26	7.72	3.74
Th	2.34	0.516	2.04	1.00	2.19	0.758
U	21.3	3.29	6.35	3.16	13.8	3.23

Table 1 (*continued*)

DSDP (site-hole)	69–504	69–504	9–84	9–84	Bulk upper hemipelagic unit	Bulk lower carbonate unit
Sample (core-section)	17H-3	52H-1	4R-4	24R-3		
Core depth (m.b.s.f)	80	230	27	210		
Description	Siliceous-nannofossil ooze	Siliceous-nannofossil chalk	Radiolarian-nannofossil ooze	Radiolarian-nannofossil chalk		
Depth in core (min) [cm]	65	60	10	120		
Depth in core (max) [cm]	70	65	15	125		
Isotopic compositions[c]						
$^{87}Sr/^{86}Sr$	0.708838 (9)	0.708935 (7)	0.708516 (7)	0.708904 (8)	0.708677	0.708920
$^{206}Pb/^{204}Pb$	18.8448 (8)	18.8504 (8)	18.8877 (8)	18.8331 (8)	18.8663	18.8417
$^{207}Pb/^{204}Pb$	15.6170 (7)	15.6031 (6)	15.6135 (10)	15.6003 (8)	15.6153	15.6017
$^{208}Pb/^{204}Pb$	38.6408 (17)	38.5581 (16)	38.7091 (22)	38.6072 (21)	38.6749	38.5804
$^{143}Nd/^{144}Nd$	0.512589 (9)	0.512647 (8)	0.512764 (7)	0.512686 (9)	0.512677	0.512667
$^{176}Hf/^{177}Hf$	0.282985 (5)	0.283074[d] (9)	0.283083 (3)	0.283074 (9)	0.282985	0.283074

[a] Major and trace element concentrations were determined by Inductevely Coupled Plasma Mass Spectrometry (ICP-MS) using a Thermo iCap-Qc at Centro de Geociencias, UNAM. All samples were initially digested in high pressure Parr bombs. Reproducibility of trace element data is given by the average concentrations and standard deviations of multiple digestions of US Geological Survey rock standards AGV-2, BHVO-2, BCR-2 and Geological Survey of Japan JB-2.

[b] Contents obtained from the DSDP initial reports from Shipboard Scientific Party on Leg 69 and 9.

[c] Isotope ratios were measured using a Thermo Neptune Plus multicollector ICP-MS at Centro de Geociencias (CGEO), UNAM. Sample preparations for isotopic analyses were performed at the clean lab facilities lab facilities of CGEO following chemical procedures described in Gómez-Tuena et al. (2014a, 2014b) and Straub et al. (2015). The values reported in the table are not age corrected and are taken as initials. 2σ mean errors (n = 80) for individual measurements are multiplied by 10^6 for Sr, Nd and Hf and by 10^4 for Pb isotopic ratios.

[d] Hf values from core 69-52H are taken from 84-24R. Chromatography separation for Hf in sample 69-52H was not possible due to initial lack of Hf in sediment sample.

Sample preparations for isotopic analyses were performed at the clean lab facilities of CGeo following chromatography ion-exchange element separation using chemical procedures described in Gómez-Tuena et al. (2014b) and Straub et al. (2015). All samples were first digested using high-pressure bombs. Isotopic ratios were measured using a Thermo Neptune Plus multi-collector ICP-MS at CGeo (Table 1: DSDP sediments; Appendix B: volcanic rocks). The measured $^{87}Sr/^{86}Sr$ ratios were corrected for mass bias to an $^{86}Sr/^{88}Sr = 0.1194$ and adjusted to a NIST SRM 987 standard ratio of $^{87}Sr/^{86}Sr = 0.710230$. During three separate intervals of analysis, the average measured $^{87}Sr/^{86}Sr$ for SRM 987 was 0.710288 ± 0.000007 (2σ, n = 8), 0.710318 ± 0.000018 (2σ, n = 9) and 0.710300 ± 0.000011 (2σ, n = 5). The measured $^{143}Nd/^{144}Nd$ ratios were corrected for mass bias to $^{46}Nd/^{144}Nd = 0.72190$ and adjusted to a JNdi standard $^{143}Nd/^{144}Nd = 0.512115$ (Tanaka et al., 2000). During three separated intervals of analyses, the average measured for $^{143}Nd/^{144}Nd$ JNdi values were 0.512099 ± 0.000004 (2σ, n = 7), 0.512103 ± 0.000005 (2σ, n = 6) and 0.512099 ± 0.000019 (2σ, n = 9). The Pb isotopic compositions were corrected for mass bias by spiking all samples with SRM 997 Tl solution with a reference $^{205}Tl/^{203}Tl = 2.3871$; and adjusted to the NIST SRM-981 standard values of $^{206}Pb/^{204}Pb = 16.9356$, $^{207}Pb/^{204}Pb = 15.4891$, $^{208}Pb/^{204}Pb = 36.7006$ (Todt et al., 1996). The average measured Pb isotopic compositions of the NIST SRM-981 were $^{206}Pb/^{204}Pb = 16.9318$, $^{207}Pb/^{204}Pb = 15.4852$ and $^{208}Pb/^{204}Pb = 36.6805$ (2σ = 44, 57, 90 ppm, respectively, n = 8), $^{206}Pb/^{204}Pb = 16.9303$, $^{207}Pb/^{204}Pb = 15.4835$ and $^{208}Pb/^{204}Pb = 36.6742$ (2σ = 50, 62, 81 ppm, respectively, n = 6), and $^{206}Pb/^{204}Pb = 16.9313$, $^{207}Pb/^{204}Pb = 5.4849$ and $^{208}Pb/^{204}Pb = 36.6782$ (2σ = 28, 31, 41 ppm, respectively, n = 7). The measured $^{176}Hf/^{177}Hf$ ratios were corrected for mass bias using $^{179}Hf/^{177}Hf = 0.7325$ and further adjusted to a $^{176}Hf/^{177}Hf = 0.282160$ of the Hf-Spex standard, which has been intercalibrated and considered identical to the JMC-475 standard (Straub et al., 2015). During the course of this study, the average measured value of the Hf-Spex was $^{176}Hf/^{177}Hf = 0.282150 \pm 0.000005$ (2σ, n = 22). Reproducibility and accuracy of the isotopic measurements were verified using U.S. Geological Survey (USGS) standards BCR-2, BHVO-2 and AGV-2, which were prepared and measured using the same procedures as the samples. Results on these standards are within analytical uncertainty to the preferred values published in the GEOREM database (http://georem.mpch-mainz.gwdg.de/) and are reported in Appendix C.

5. Results

5.1. Petrography

The studied rocks from NSI are porphyritic andesites and show a mineral assemblage dominated by plagioclase + clinopyroxene + orthopyroxene with variable small contents of amphibole, olivine and biotite; characteristics also found in other eruptive centers within the NVP (Martínez et al., 2014). Plagioclase is present as a matrix aggregate in tiny laths displaying a trachytic texture, and as a phenocryst showing disequilibrium features such as sieve textures, mineral overgrowths, complex zoning and corroded rims. Orthopyroxene and clinopyroxene are mainly phenocrysts of fine (<1 mm) to medium-grained (up to 4 mm) size and are often associated with glomeroporphyritic aggregates that also include plagioclase (Fig. 3a), and in some rare cases amphibole and biotite. Orthopyroxene tends to show disequilibrium textures such as corroded rims and clinopyroxene or amphibole coronas. Amphibole is fine to medium-grained and commonly displays opacitic rims or is completely oxidized by devolatilization. In these rocks, and generally along the NVP, olivine is common as xenocrysts, showing rims of clinopyroxene and amphibole. Nonetheless, we report olivine-phyric lava flows that contain up to 10% modal, fine to medium-grained size (up to 3 mm) olivine (Fig. 3b). These phenocrysts do not show disequilibrium textures or dissolution and in some rare cases were found as glomeroporphyritic aggregates.

CMV also produce porphyritic rocks but is distinguished by a mineralogical assemblage made of plagioclase + amphibole + biotite and minor amounts of quartz, pyroxene and olivine (Fig. 3c–d). Plagioclase is present aggregates in the matrix and as phenocrysts showing complex zoning and overgrowths, of up to 4 mm. Amphibole and biotite are present as fine to medium-grained size (Fig. 3c–d) (0.5-2 mm) and in some occasions as glomeroporphyritic aggregates (Fig. 3c). Among the studied rocks we find no evidence of intense alteration due to weathering or to hydrothermal fluids, which is evident in the intact preservation of the mineralogical phases of the studied rocks.

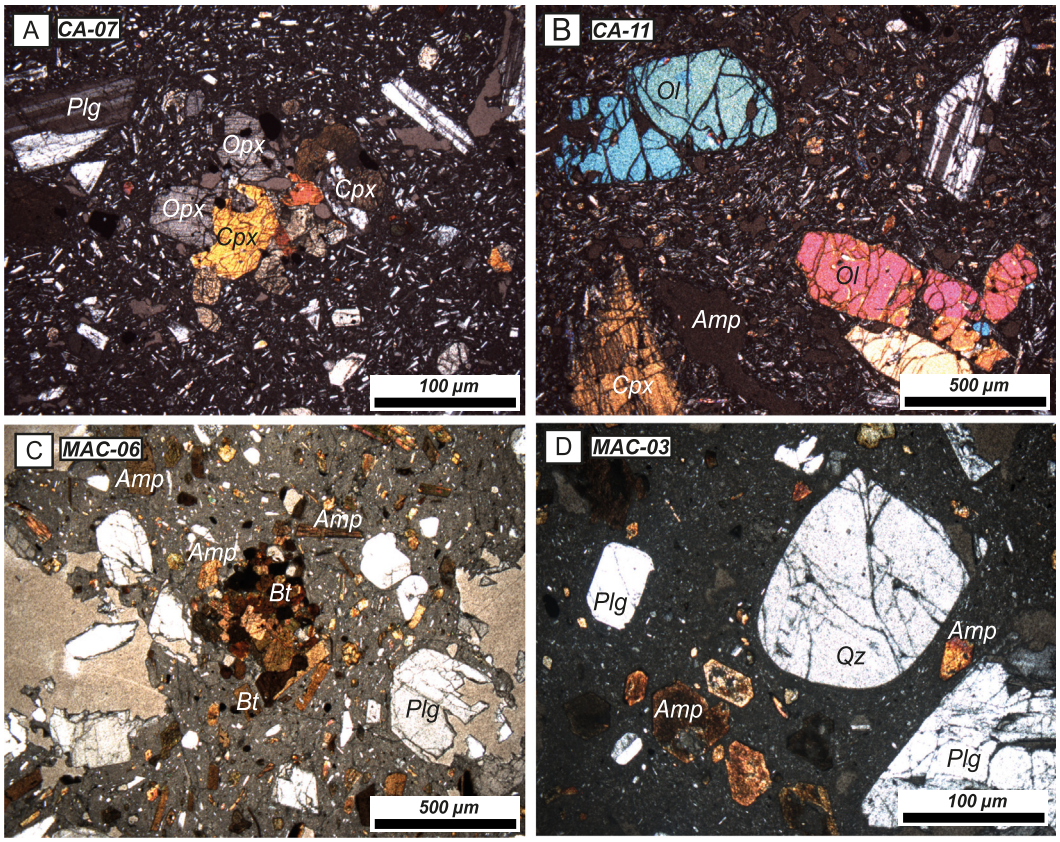

Fig. 3. Representative thin section photographs for NSI and CMV lava flows and domes. (A) Common glomeroporphyric aggregates of ortho- and clinopyroxene found in andesitic NSI lavas. Matrix microcrysts consists of plagioclase and pyroxene laths. (B) Olivine phenocrysts commonly found in the most primitive NSI lavas. (C) Glomeroporphyric aggregates of amphibole and biotite from CMV lava domes. Matrix microcrysts also exhibit this mineral assemblage (D) Quartz phenocryst, plagioclase and amphibole are the common mineralogical assemblages in CMV lava dome.

5.2. Major and trace element geochemistry

The studied volcanic rocks display a narrow range of compositions spanning between andesites, trachyandesites and dacites with SiO_2 contents between 58.2 and 66.87 wt% (Fig. 4a). The alkaline elements ($Na_2O + K_2O$) are variable between eruptive centers, although both NSI and CMV belong to the sub-alkaline series (Macdonald and Katsura, 1964) (Fig. 4a). In the SiO_2 vs. K_2O diagram (Peccerillo and Taylor, 1976), NSI rocks fall in the high-K calc-alkaline field, while CMV rocks display lower K_2O contents plotting in the low-K calc-alkaline field (Fig. 4b). Rocks from NSI are overall similar to Nevado del Ruiz in terms of the major elements, albeit they are slightly more enriched in K_2O. Both NSI and CMV show high and homogeneous Mg# (molar Mg# = 100*MgO/[FeO* + MgO]) from 55.2 to 68.3 across the SiO_2 variability (see Fig. 4c). As it is usually observed in arc magmas (Gill, 1981), NSI and CVM display linear trends in major element diagrams with respect to SiO_2 (Fig. 5). Yet, some important differences are observed between NSI and CMV products in terms of their relative major element abundances. Rocks from NSI are less evolved, but they follow an evolutionary trend to higher Al_2O_3 contents and lower CaO, TiO_2, MgO and Fe_2O_3 with respect to CMV, whereas the Na_2O contents are more or less equivalent in both volcanoes (Fig. 5).

The trace element patterns of the studied rocks show typical characteristics of continental volcanic arc products, such as high ratios of Large Ion Lithophile Elements (LILE) over Heavy Rare Earth Elements (HREE), incompatible element enrichments, negative Nb-Ta anomalies and positive spikes in Pb and Sr (Fig. 4c). And yet, the two volcanoes display subtle variations in their relative trace element abundances. Rocks from NSI are distinguished by their higher U (4–6) and Th (7.5–13) concentrations, and their lower Nb/Ta (~12) and MREE/HREE ratios (Fig. 4d). These trace element characteristics are also observed in rocks from nearby Nevado del Ruiz volcano, indicating that equivalent petrogenetic processes may operate in both volcanoes. In contrast, and despite its more evolved character, CMV products are characterized by lower concentrations of highly incompatible trace elements like U (~2) and Th (6–7), and also extend to higher Nb/Ta (~16) and MREE/HREE ratios (Fig. 4d).

5.3. Isotope geochemistry

The two volcanoes also display distinct Sr-Nd-Pb-Hf isotopic compositions (Fig. 6). Overall, rocks from the NSI have a relatively more depleted character in their Sr, Nd and Hf isotopic compositions when compared to CMV (Fig. 6a and d). For the Pb isotopic systems, however, rocks from CMV show slightly more radiogenic values in $^{207}Pb/^{204}Pb$ and $^{208}Pb/^{204}Pb$ ratios than NSI at nearly equivalent $^{206}Pb/^{204}Pb$ values (Fig. 6b and c, respectively). Therefore, the two volcanoes plot towards different end-member compositions in the $^{206}Pb/^{204}Pb$ vs. $^{207}Pb/^{204}Pb$ diagram (Fig. 6b, see inset) even if they appear to follow a single mixing line in the $^{207}Pb/^{204}Pb$ vs. $^{208}Pb/^{204}Pb$ variation diagram (not shown). In Nd-Hf isotopic space (Fig. 6d), CMV has more radiogenic values that plot close to the so-called "terrestrial array" (Vervoort et al., 1999), whereas NSI is less radiogenic and displays variable $^{143}Nd/^{144}Nd$ at almost constant $^{176}Hf/^{177}Hf$ values, following a trend that somehow parallels the so-called "seawater array" (Albarède et al., 1998). For comparison, rocks from the SVP (see Marín-Cerón et al., 2010) are slightly more depleted than the NVP in terms of Sr-Nd (Fig. 6a), have more enriched and variable Pb isotopic compositions (Fig. 6b), and do not exhibit a positive correlation on Pb-Sr isotopic space (Fig. 6c). For the Hf isotopic compositions, the SVP also displays quite variable isotopic values that are in general more depleted than the NVP.

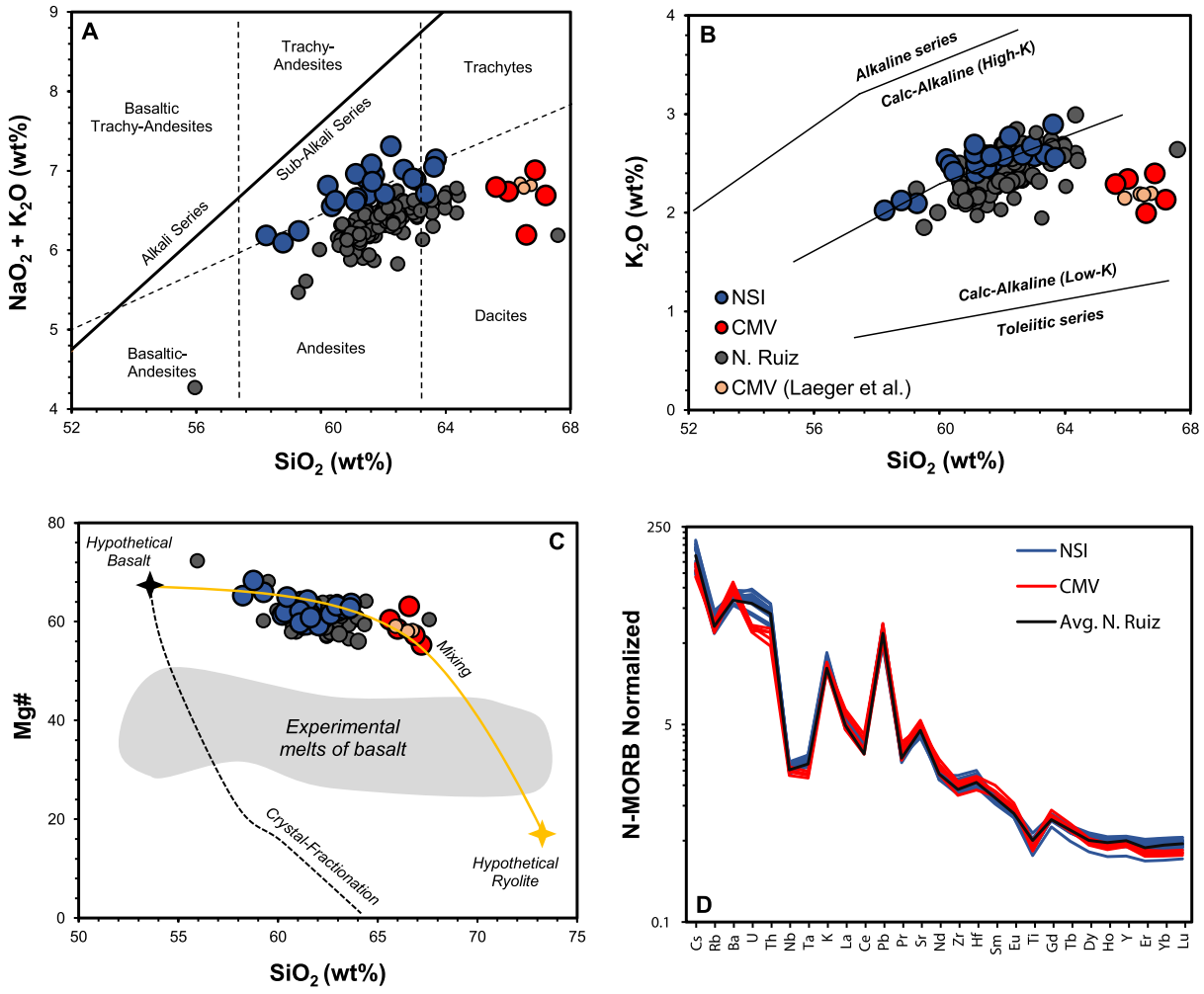

Fig. 4. Mayor and trace element variation diagrams of the studied volcanoes. (A) Total alkalis vs. silica diagram (Le Maitre et al., 2002). (B) K_2O vs. SiO_2 diagram (Peccerillo and Taylor, 1976). (C) Mg# (Mg# = 100*MgO/[FeO* + MgO]) vs. SiO_2. Both NSI and CMV show high Mg# throughout the SiO_2 variation. The dotted line denotes a typical crystal fractionation path of an arc basalt from the Trans-Mexican Volcanic Belt (Gómez-Tuena et al., 2014b). The rapid drop in #Mg is mainly caused by the early crystallization of olivine and pyroxene. The yellow line denotes a simple mixing model between a hypothetical rhyolite and a basalt. (D) Multi-element plot of the studied rocks normalized to N-MORB (Gale et al., 2013). Main differences between NSI and CVM are observed in Th and U concentrations, Nb/Ta ratios and the REE patterns. Also shown are data from CMV (Laeger et al., 2013) and Nevado del Ruiz (Martínez et al., 2014). It is worth noting that although we did not measure SiO_2 directly, normalization to 100% for all major elements adequately reproduce the SiO_2 values reported elsewhere in the same eruptive center (CMV) and from compositionally similar nearby volcanoes (NSI and Nevado del Ruiz).

Fig. 6 also shows the isotopic compositions of relevant crustal components of the Northern Andes in comparison to potential subduction inputs. On a broad picture, NVP rocks plot between the composition of the Nazca Equatorial Pacific Ridge (EPR) (Gale et al., 2013) and a crustal component that could be represented by sediments from the Atlantic or the Pacific oceans, which themselves display contrasting isotopic compositions. The Atlantic sediments are isotopically more enriched than the Pacific sediments offshore Colombia. On the other hand, the Paleozoic metamorphic basement upon which the NVP is emplaced displays low Nd and Sr isotopic values and a distinct array in the $^{206}Pb/^{204}Pb$ vs. $^{207}Pb/^{204}Pb$ isotopic space that differs from that of the Quaternary volcanoes (Cochrane et al., 2014). The lower crustal xenoliths have similar Sr isotopes than the volcanoes, but extend to higher Nd and Pb isotopic compositions than the Paleozoic basement (Weber et al., 2002) (Fig. 6a, b and c).

6. Discussion

In this section, we will evaluate the different hypotheses that have been put forward to explain the geochemical characteristics of the studied eruptive centers, incorporating new geochemical data for the volcanic products and the potential subduction components involved. Our aim is to provide a new model for the formation of the NVP that may help explain the geochemical diversity observed throughout the studied area, within the geodynamic setting of the Northern Colombian Andes.

6.1. Testing intra-crustal differentiation and contamination processes

To the date, no investigations have taken into account the geochemical variability of the NVP as a whole, but some compelling ideas have been put forth to explain the petrogenesis of specific eruptive centers. One of the first hypotheses was presented by James and Murcia (1984) for Nevado del Ruiz which proposed an assimilation-fractional crystallization model of a mantle derived melt that incorporated 10%–20% of crustal material. Later studies have suggested that the geochemical variability of Nevado del Ruiz volcano is related to simple crystal fractionation of an enriched mantle-derived basalt with negligible crustal contamination (Vatin-Pérignon et al., 1988; Vatin-Pérignon et al., 1990). In recent years, petrologic models concerning the "adakitic" and enriched isotopic nature of CVM (Laeger et al., 2013) have been associated to intra-crustal melting, mixing and homogenization of lower crustal lithologies with a mantle-derived basalt, following a Crustal Hot Zones model (Annen et al., 2006).

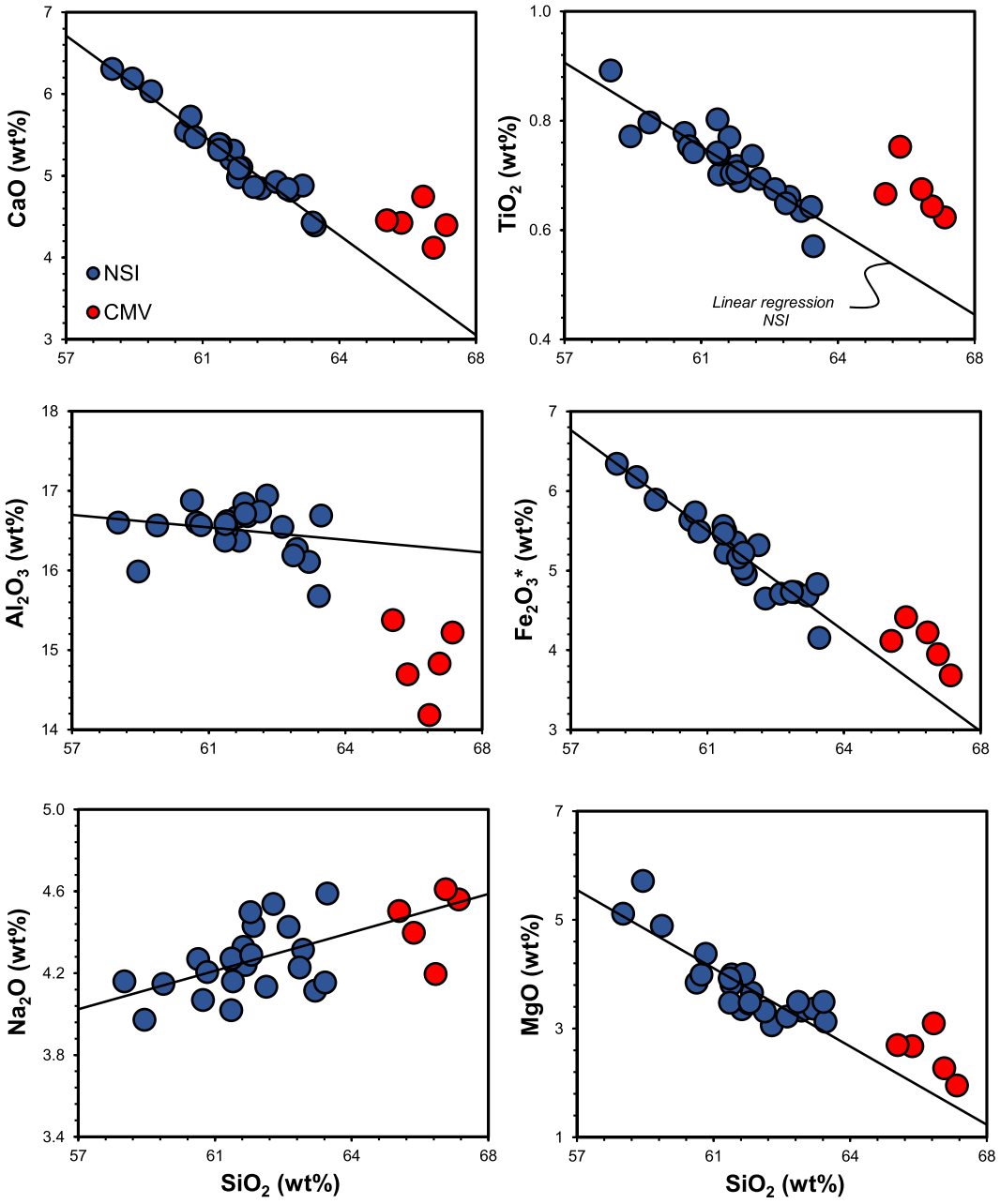

Fig. 5. Major element variation diagrams with respect to SiO_2. NSI rocks show linear trends without any major element inflection. Regression lines along the NSI data indicate that products of CMV and NSI do not follow the same evolution.

Differentiation processes operating in the overriding crust from a common basaltic precursor are recurrently invoked in the literature, and yet the homogeneously high Mg# of calc-alkaline andesites and dacites cannot be easily explained by crystallization or contamination processes because fractionation of olivine and/or pyroxene, an assemblage commonly found in basaltic rocks, will rapidly decrease the Mg#, even at low SiO_2 contents (Gómez-Tuena et al., 2014b; Kelemen, 1995) (see Fig. 4c, dashed line). Direct melting of a basaltic precursor would also create derivative liquids with low Mg# that are unlike those observed in NVP andesites (Fig. 4c) (Rapp, 1995; Sen and Dunn, 1994). Instead, the linear trends displayed by the major elements and the relative constant Mg# at variable SiO_2 contents (Figs. 4 and 5), appear to be consistent with a mixing process between felsic and mafic components. Indeed, rocks from CMV have been argued to be formed by a mixture between a mantle-derived basaltic precursor and a differentiated silicic melt formed in lower crustal magma reservoirs (Laeger et al., 2013). Nonetheless, if processes like these are pervasive along the NVP, why is it that volcanoes like NSI and CVM display such contrasting geochemical characteristics?

Because the HREE and High Field Strength Elements (HFSE) are largely insoluble elements, their relative concentrations in magmatic rocks are essentially controlled by the presence or absence of certain mineral species that strongly partition them, such as amphibole, garnet or rutile (Gómez-Tuena et al., 2011; Green, 1995). Therefore, evaluating the distinct features between the two rock groups in terms of their HREE and HFSE ratios may help elucidate the characteristics of their fractionation assemblages (Fig. 7). Rocks from NSI, for example, display low Dy/Yb values (Fig. 7a) that have been traditionally attributed to melting in the presence of amphibole (Davidson et al., 2007), given the stronger partitioning of the MREE over the HREE in the amphibole structure (Bottazzi et al., 1999). In contrast, rocks from CMV show higher Dy/Yb values, probably indicating the presence of residual garnet in the source

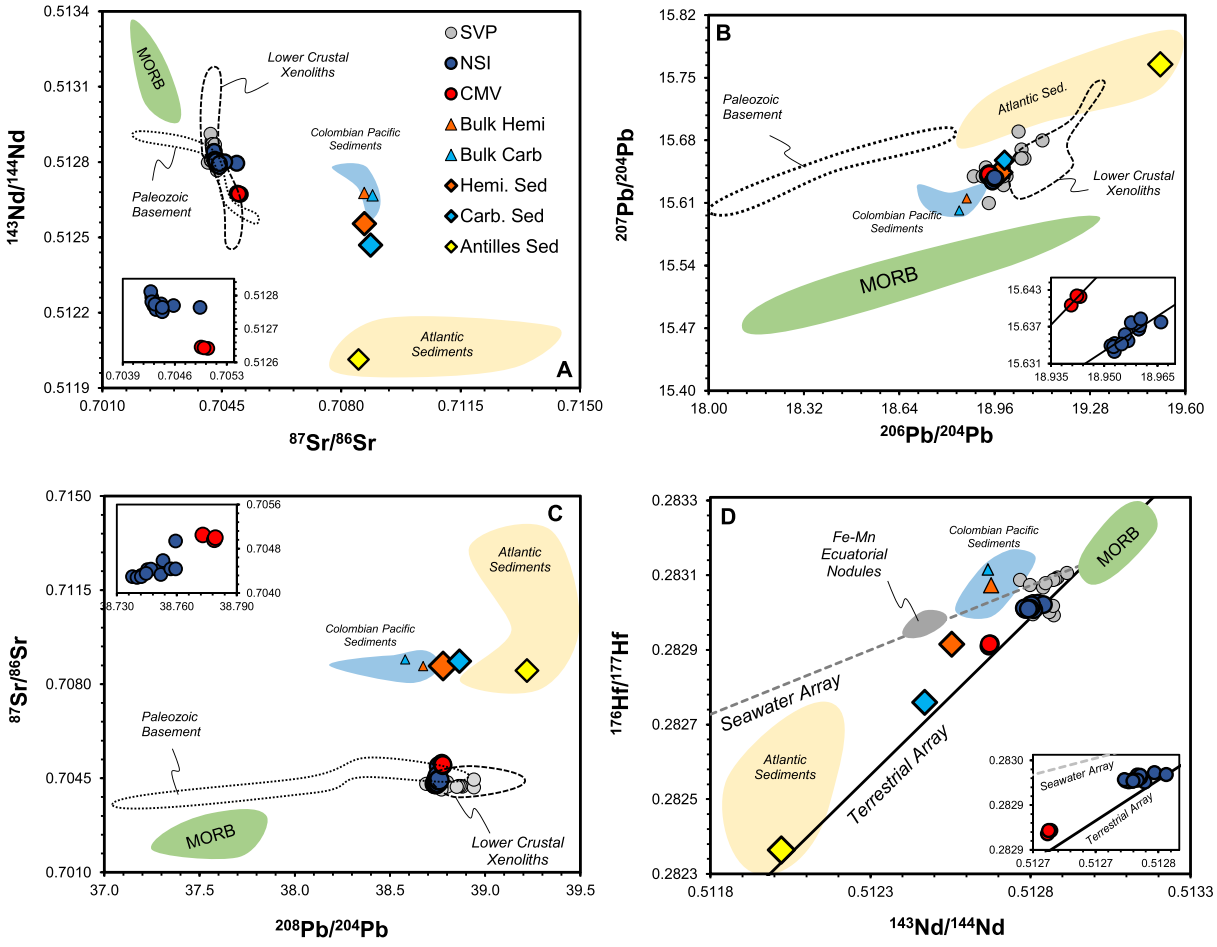

Fig. 6. Isotopic systematics of the studied volcanoes and other possible end-members. (A) $^{87}Sr/^{86}Sr$ vs. $^{143}Nd/^{144}Nd$. (B) $^{206}Pb/^{204}Pb$ vs. $^{207}Pb/^{204}Pb$. (C) $^{208}Pb/^{204}Pb$ vs. $^{87}Sr/^{86}Sr$. (D) $^{143}Nd/^{144}Nd$ vs. $^{176}Hf/^{177}Hf$. Black line denotes the "Terrestrial Array" according to Vervoort et al. (1999), the gray dotted line denotes the "Seawater Array" according to Albarède et al. (1998). Equatorial Pacific Nodules from van de Flierdt et al. (2004). Also shown in all figures: MORB data from Gale et al. (2013); lower crustal xenoliths from the Northern Andes (Weber et al., 2002); South Volcanic Province of Colombia from Marín-Cerón et al. (2010); Paleozoic basement of the NVP (Cochrane et al., 2014), Pacific Colombian Sediments from the DSDP 69 and 84 offshore Colombia (this study; Table 1), Atlantic sediment field from SedDB (www.earthchem.org/seddb) and Lesser Antilles sediments site 144 from Carpentier et al., 2009. Diamonds for Hemipelagic and Carbonate sediment are mixtures of Atlantic and Pacific sediments (see Discussion).

(Davidson et al., 2007), because garnet has a higher compatibility of the HREE over the MREE (Johnson, 1994). Moreover, NSI display high Ta/Nb ratios (Fig. 7b, inset) that are analog to the modern continental crust (Green, 1995; Rudnick, 2000) and similar to those observed in experimental studies where amphibole appears as a residual phase (Rapp and Watson, 1995). Rocks of CMV show lower Ta/Nb ratios (Fig. 7b, inset) suggesting that rutile, instead of amphibole, might be the main residual phase, given the higher compatibility of Ta over Nb in the rutile structure in silicate melts (Green, 1995; Rapp et al., 2003). In summary, these contrasting trace element characteristics indicate that an amphibole-rich residual assemblage may be controlling the trace element fractionations of NSI products, whereas a rutile-bearing eclogitic high-pressure assemblage appears to be governing the REE and Nb/Ta systematics of CVM.

These kinds of geochemical variations, and especially the distinct REE patterns, have been related to intra-crustal differentiation at different depths (Chiaradia, 2015), but also to subduction-driven mechanisms related to slab melting (Defant and Drummond, 1990) or to different mineral assemblages in the mantle source of arc volcanoes (Alonso-Perez et al., 2009). Recent geophysical studies (Poveda et al., 2015; Poveda et al., 2018; Yarce et al., 2014) have shown that CMV is indeed emplaced on a slightly thicker crust (~52 km; 15 kbar) than NSI (~45 km; 13 kbar), suggesting that a garnet-rich higher-pressure residual assemblage could account for CMV REE systematics. In spite of that, experimental studies have shown that garnet and amphibole could be both stable at those lithospheric pressures (Alonso-Perez et al., 2009; Schmidt and Poli, 2013), indicating that other features, like water content, exert a stronger control on the residual assemblage rather than pressure alone. Indeed, Zellmer et al. (2012) have argued that dryer melts will enhance garnet stability even at relatively shallow crustal depths (40–30 km). Although no hygrometers have been applied along the NVP, rocks from CMV show larger modal quantities of biotite and amphibole than NSI, an assemblage that is otherwise consistent with the ~7% H_2O contents determined using thermo-barometric formulations (Laeger et al., 2013). This clearly indicates that CMV could be even more hydrous than NSI and thus rules out the possibility of an important H_2O control on garnet vs. amphibole formation below the studied volcanoes.

Fig. 7 also shows that other incompatible trace element ratios like Th/Nb and Th/La in the studied volcanoes are also decoupled following different mixing lines. They depart from the compositions of the lower crustal xenoliths or a MORB-like component and extend to distinctly enriched end-members with higher Th/Nb and Th/La ratios, and radiogenic Pb isotopic compositions. If this decoupling is controlled by differentiation processes at depth (Rudnick, 1995), then the crust would not only need to be compositionally different below the two volcanoes, but also different from the composition of the local Paleozoic basement (Fig. 6b), and even distinct from the lower crustal xenoliths that are considered to be representative of the deep crust in the region. These xenoliths display extremely low Th contents (see Weber et al., 2002)

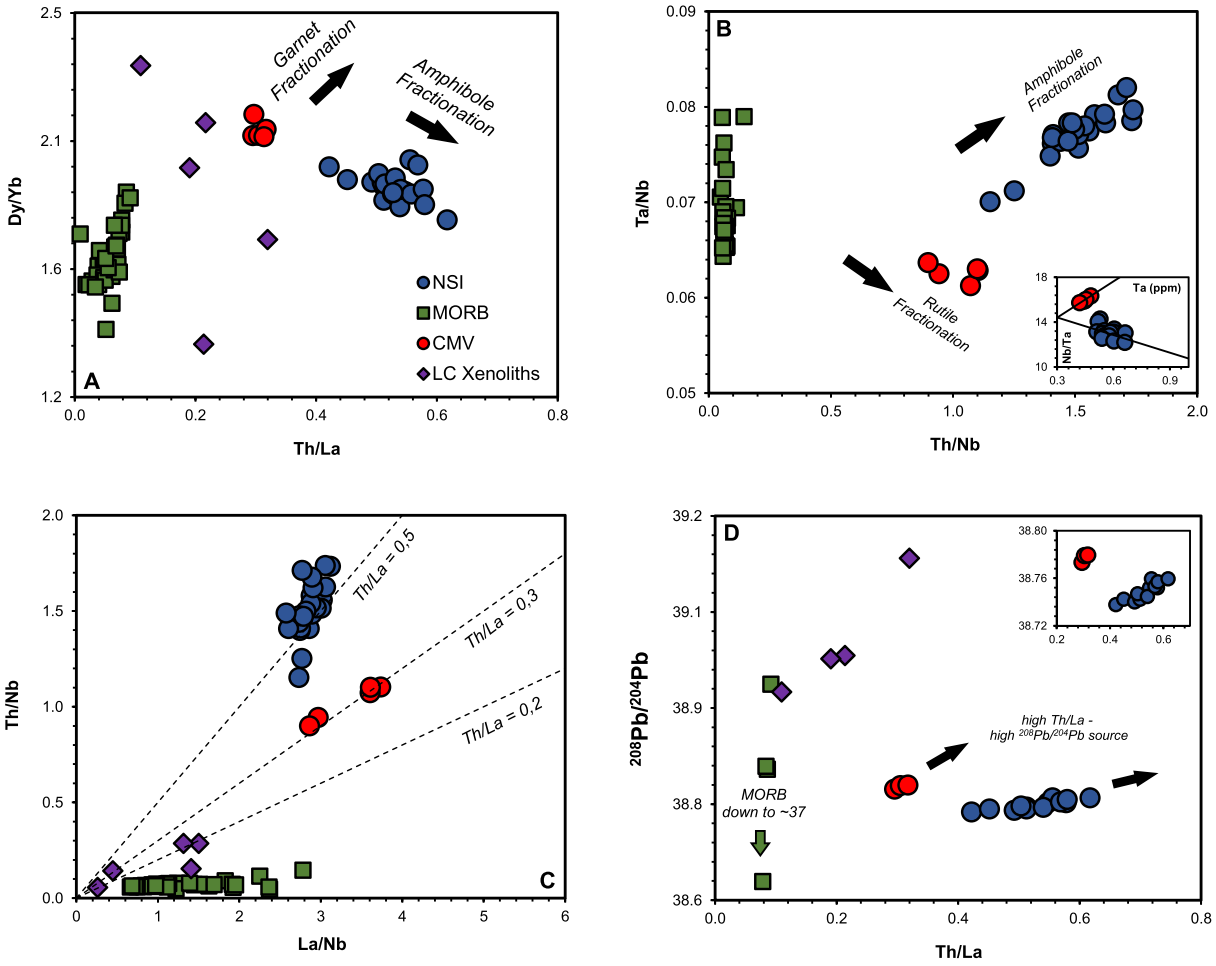

Fig. 7. Trace element and isotopic diagrams for discriminating crustal contamination (see Discussion). (A) Dy/Yb vs. Th/La. Systematics observed in NSI and CMV products taken from Davidson et al. (2007). (B) Ta/Nb vs. Th/Nb and Ta vs. Nb/Ta (inset). (C) La/Nb vs. Th/Nb and Th/La values for both NSI and CMV rocks. (B) Th/La vs. $^{208}Pb/^{204}Pb$. High Th/La ratios from the NVP rocks correlate with Pb isotopic enrichments. Also shown: MORB data from Gale et al. (2013) and data from lower crustal xenoliths from Weber et al. (2002).

and thus lower Th/La ratios than those required to explain the high Th/La ratios and the Pb isotopic compositions of the volcanoes (Fig. 7c–d). Since the two enriched end-members cannot be controlled by melting of a homogeneous lower crust, and neither can they be formed by crystal fractionation of a common crustal source (see Plank, 2005), we argue that the compositional differences should be then acquired by different components being fed to the source of these two volcanoes deep in the subduction zone.

6.2. The Colombian Pb paradox and the possible contributions from Atlantic sediments

Before we evaluate the role of the subducted lithologies in the petrogenesis of the NVP, we will first address the origin of the enigmatic Pb isotopic compositions of the studied volcanic arc products.

South of the study area, in the Northern Andes of Ecuador, the Pb isotopic compositions of Quaternary volcanoes have been related to either crustal contamination with the local basement (Nauret et al., 2018), to variations in the mantle region due to different metasomatic agents (Ancellin et al., 2017) or to pre-subduction mantle heterogeneity (Chiaradia and Fontbote, 2002). Similarly, in the SVP of Colombia, the radiogenic Pb isotopic compositions were interpreted by Marín-Cerón et al. (2010) to be acquired by assimilation of the lower crust of the SVP studied by Weber et al. (2002). In contrast, in the Central American arc, the Pb isotopic compositions have been explained as contributions from tectonically eroded forearc lithologies of the accreted Caribbean Large Igneous Province (CLIP) (Goss and Kay, 2006).

While it is clear that all the aforementioned components may also play a role in the petrogenesis of the Colombian Andes, when viewed in detail, however, none of them can explain the radiogenic end-member component required by the Pb isotopic mixing array displayed by the volcanoes. When all Eastern Pacific sediments are considered, for example, no enriched end-member appears to be close to trend or overlap the NVP rocks (Fig. 8a). Furthermore, the isotopically enriched end-member cannot be explained by forearc subduction erosion, because NVP and SVP rocks display much higher $^{207}Pb/^{204}Pb$ values (Fig. 8a) than the forearc CLIP-like lithologies of Colombia and Central America (Kerr et al., 1997). As discussed above, melting or assimilation of the lower crust would not be able to create an adequate end-member having both, diverging Th/La ratios and radiogenic Pb isotopes at the same time (Fig. 7d). The studied Pacific sediments offshore Colombia are also inadequate because they have similar Pb compositions from the Eastern Pacific sediments. Different mantle reservoirs also plot away from the main trend displayed by the Colombian volcanoes. Consequently, no mantellic, crustal or subducted material analyzed so far within the present-day Equatorial-Pacific configuration can be used to explain the radiogenic Pb isotopic compositions of these North Andean volcanic rocks.

Taking this evidence into consideration, we investigated the possibility that sediments with compositions similar to those currently deposited in the Atlantic basin could have been involved in the petrogenesis of the NVP. The Atlantic sediments extend to more enriched Pb and Hf isotope values than those from the Pacific basin, and therefore they can provide an adequate end-member for the mixing

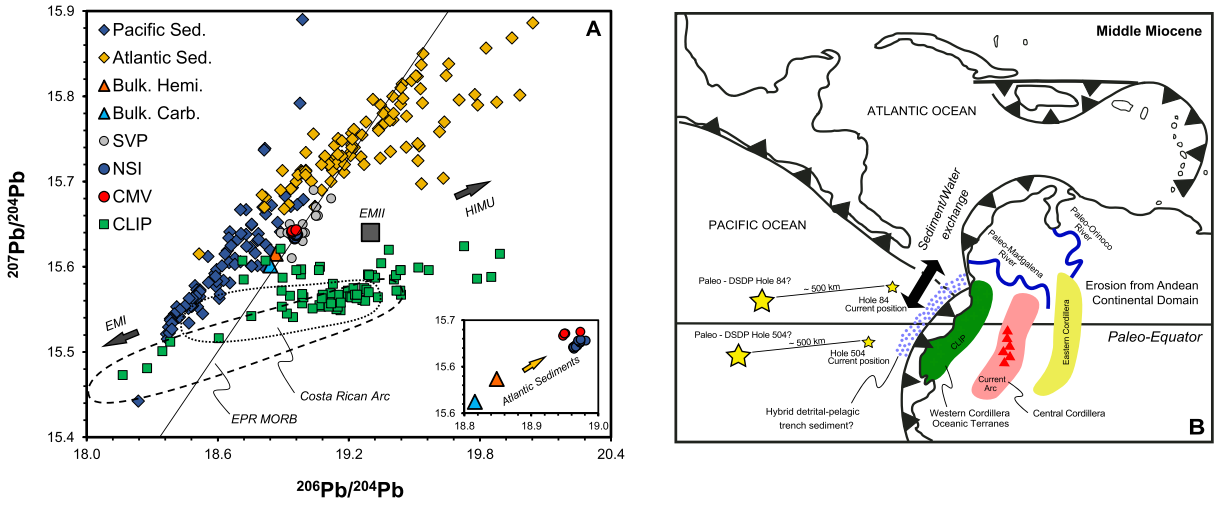

Fig. 8. (A) Pb isotopic compositions of the Caribbean Large Igneous Province (CLIP) and accreted terrains from Central America and Colombia (Kerr et al., 1997), Eastern Pacific sediments and Atlantic sediments from SedDB (www.earthchem.org/seddb), Costa Rican arc lavas from Goss and Kay (2006), bulk hemipelagic and carbonate sediment from Table 1, South Volcanic Province (SVP) from Marín-Cerón et al. (2010) and mantle reservoirs from Workman et al. (2004) and references therein. SVP and NVP rocks do not plot towards the CLIP field, the Pacific sediments or enriched mantle reservoirs, indicating that these components alone cannot explain the NVP isotopic systematics. (B) Middle Miocene Paleo-reconstruction for the Pacific - Atlantic Junction prior to the closure of the Central American Seaway. Paleo continental margin contours from Pindell and Kennan (2009). Locations of DSDP Sites were constrained using the current absolute motion of the Nazca Plate (Syracuse et al., 2010). Western Cordillera terrains were already above sea level during the middle Miocene (Villagómez et al., 2011), limiting the continental detrital erosion from the continental domain from Eastern and Central Cordillera. Atlantic and Pacific Oceans had water inter-connection during the middle Miocene times. This sediment/water exchange between the two oceans could have result in a hybrid trench sediment which was subducted between 7 and 8 Ma.

relationships (Fig. 8). Is it possible that sediments coming from so distant sources could have been mixed together in the past before being subducted along the Colombian trench?

Several lines of evidence - from paleographic reconstructions (Pindell and Kennan, 2009) to biological and genetic similarities among equatorial Atlantic and Pacific faunas (Bacon et al., 2015) and even paleoclimate records (Molnar, 2008) - suggest that prior to the closure of the Central American seaway and the formation of the Panama Isthmus, in the Late Miocene, the Atlantic and Pacific basins shared a common oceanographic past. Numerical models have also predicted a westward incursion of surface Atlantic waters into the Pacific prior to the formation of the Panama Isthmus (Nof and Van Gorder, 2003). Based on this evidence, Fig. 8b shows a possible paleographic and tectonic reconstruction for the Equatorial Americas during the Middle Miocene. At that time, sediments derived from the Western Cordillera of Colombia, which is constituted by CLIP accreted terranes, were already draining to the Pacific basin (Villagómez et al., 2011), and thus blocking detritus coming from the continental interior to reach the Pacific. However, and even though most riverine basins washing the continental interior were draining to the Atlantic as they do today, the paleo-Magdalena river had westward depocenters delivering continental detritus close to the paleo-Pacific trench (Villamil, 1999). All of this evidence suggests that the interconnection of Atlantic and Pacific waters and sediments prior to the closure of the Central American seaway could have resulted in a hybrid trench sediment with particular features akin to both sources.

6.3. The reconstructed sediment component

Considering the current subduction rates of 60 mm/year along the Colombian margin (Syracuse et al., 2010), we estimate that it would take between 5 and 7 My for a subducted sediment to be transported inboard to the longitude of the NVP. Thus, the sedimentary components potentially contributing to the arc volcanoes were probably subducted in the latest Miocene. Because DSDP Sites 69 and 9 outboard Colombia would have been located ~500 km to the west of its present location at that age, the Miocene age sediments at the base of the columns are not recording any significant detrital contribution coming from the continental margin. Likewise, the youngest post-Pliocene sedimentary layers of the upper sections would not be able to register any potential contribution from Atlantic sediments because the Panama Isthmus was already established by that time. For these reasons, and in order to satisfy the Nd-Hf-Sr and Pb-Pb (Figs. 6 and 8) isotopic mixing relationships displayed by the studied volcanoes, we modulated the trace element and isotopic compositions of the two main lithologies sampled at the DSDP Sites, assuming small contributions from an Atlantic sediment. This results in a hemipelagic and carbonate Colombian trench sediment (Table 1) hybridized with about 12% contribution from an Atlantic sediment (Table 2). We assume that the Atlantic sedimentary contribution is compositionally similar to the bulk composition of DSDP Site 144 from the Lesser Antilles (Carpentier et al., 2009). These sediments represent the erosional products of the Eastern Cordillera of Colombia transported by the Orinoco River, and thus provide a good proxy of the eroded lithologies in the paleo-Magdalena watershed (Fig. 8b). The compositions of the hybrid bulk sediments do not greatly differ from the originals in most trace element abundances or Sr isotopes because the Colombian Pacific sediments are already highly enriched when compared to the Atlantic sediments (see Figs. 9 and 10). Nonetheless, the Pb and Hf abundances and their isotopic ratios will be more strongly affected by the terrigenous contributions from the Atlantic sediments because the carbonate-rich Pacific sediments have lower Pb and Hf contents.

6.4. Elemental transport from sediments to arc rocks

Geochemical studies of global arcs have demonstrated a strong connectivity between subduction inputs and volcanic outputs (Plank and Langmuir, 1993). It has been shown that arc rocks mostly inherit their high LILE/HFSE ratios and their radiogenic isotopic features from the subducted trench sediments or eroded forearc debris (Elliott et al., 1997; Parolari et al., 2018; Patino et al., 2000; Plank et al., 2002; Straub et al., 2015). Nonetheless, the studied volcanoes have different trace element contents and isotopic compositions, and thus, follow diverging trends in several element ratio mixing plots indicating that more than two components must be involved (Fig. 9). If, as shown above, these features are not controlled by contamination with the overriding crust, they may be governed instead by the participation of different kinds of sediments entering the subduction channel.

Table 2
End-member compositions and partition coefficients used in the models.

	AOC[a]	Bulk D[b]	AOC melt[c]	Hemi. Sed[d]	Bulk D[e]	Carb. Sed[f]	Bulk D[g]
Rb	2.1	0.05	22	33	0.65	17	0.23
Ba	23	0.03	298	3862	1.50	2879	0.54
Th	0.290	0.04	3.17	2.85	0.28	1.59	0.23
U	0.100	0.05	1.00	12.8	0.56	3.43	0.70
La	4.47	0.22	17.4	15.8	2.31	11.5	1.08
Sr	320	0.19	1362	527	1.31	1014	1.42
Pb	0.460	0.14	2.97	8.09	0.32	4.67	0.12
Nd	9.36	0.69	13.2	14.5	2.34	8.86	0.74
Sm	3.78	0.67	5.51	3.15	3.94	1.74	2.47
Hf	1.38	0.69	2.00	1.92	0.82	0.902	0.39
$^{87}Sr/^{86}Sr$	0.703200		0.703200	0.708677		0.708861	
$^{206}Pb/^{204}Pb$	18.5728		18.5728	18.9730		19.0403	
$^{207}Pb/^{204}Pb$	15.5225		15.5225	15.6404		15.6547	
$^{208}Pb/^{204}Pb$	38.0844		38.0844	38.7668		38.8076	
$^{143}Nd/^{144}Nd$	0.513103		0.513103	0.512554		0.512469	
$^{176}Hf/^{177}Hf$	0.283120		0.283188	0.282884		0.282742	

[a] MORB (AOC) composition from an average Eastern Pacific Rise from Gale et al. (2013) between 10° and 0° N, considering Sr enrichment for sea water alteration.

[b] Bulk D partition coefficients of intermediate composition melts in equilibrium with an amphibolitic assablage (50% amph, 35% pxn, 15% grt). Individual Kd's values from Rollinson (1993, and references therein), Hart and Dunn (1993) and Geochemical Earth Reference Model (GERM) (http://www.earthref.org).

[c] Composition of AOC melt assuming 5% of batch melting.

[d] Hemipelagic composition base on the mean upper composite section from DSDP Site 504 and 84 outboard Colombia (Table 1) with a 12% Atlantic sediment added from bulk DSDP site 144 from the Lesser Antilles (Carpentier et al., 2009).

[e] Bulk D partition coefficients for andesitic/dacitic liquids for sediment melting considering a mineralogical assamblage base on modal abundances from the sedimentary column from site 504 (Leg 69) (Beiersdorf and Rösch, 1983) and experimental melting of carbonate lithologies (Skora et al., 2015): 18% carbonate, 40% pxn, 15% apt, 12% grt, 15% bt. Individual Kd's values for carbonate from Skora et al. (2015), apatite from Prowatke and Klemme (2006), pyroxene and biotite from Geochemical Earth Reference Model (GERM) (http://www.earthref.org).

[f] Carbonate composition base on the mean lower section from DSDP Site 504 and 84 outboard Colombia (Table 1) with a 12% Atlantic sediment added from DSDP site 144 from the Lesser Antilles (Carpentier et al., 2009).

[g] Bulk D partition coefficients for andesitic/dacitic liquids for sediment melting considering a mineralogical assamblage base on modal abundances from the sedimentary column from site 504 (Leg 69) (Beiersdorf and Rösch, 1983) and experimental melting of carbonate lithologies (Skora et al., 2015): 40% carbonate, 30% pxn, 25% grt, 5% bt. Individual Kd's values for carbonate from Skora et al. (2015), pyroxene and biotite from Geochemical Earth Reference Model (GERM) (http://www.earthref.org).

Elements like U and Th are key in evaluating the budget transport from slab to arc (Elliott et al., 1997; Hawkesworth et al., 1997; Kelley et al., 2005). Thorium is an incompatible and insoluble element that exhibits different concentrations in both sedimentary packages from the Eastern Pacific (See Plank et al., 2002 and this study). Since the Th contents of MORB and the mantle wedge are extremely low, the Th budget in arc products will be mainly controlled by the subducted sediments (Plank and Langmuir, 1998). Elements like U, Rb and Ba are also incompatible and depleted in mantle rocks when compared to the Colombian trench sediments (Gale et al., 2013; Workman and Hart, 2005), but they are also fluid-mobile elements that are heterogeneously distributed in marine sediments (see Fig. 2), and therefore, their variations in arc products may also be strongly governed by the sedimentary input (Plank, 2013; Plank and Langmuir, 1998).

A good way of testing if the subducted sediments play a role in arc magmatism is the Sm/La vs. Th/La mixing diagram (Fig. 9a). Arc rocks usually display simple mixing linear relationships between the mantle wedge and their local trench sediments in this diagram, suggesting that the Th/La ratios of arc products are inherited from the trench sediments (see Plank, 2005). Interestingly, volcanoes from the NVP also display linear mixing trends in this diagram, but they extend to higher Th/La ratios than the Colombian trench sediments or their reconstructed hybrids (Fig. 9a). The Th/La ratios of hemipelagic (0.16) and carbonate (0.01) trench sediments differ by a factor of 10, but they are still much lower than those of the volcanic products (up to 0.62). In fact, rocks from NSI have higher Th/La ratios than the global range of analyzed oceanic sediments (Vervoort et al., 2011). Because incorporating these sediments in bulk will not explain the high Th/La of these arc rocks, we conclude that, at least for the Colombian case, the Th/La ratio must be significantly fractionated during sediment melting at subarc depths.

Trench sediments provide a good geochemical proxy of the input parameters in subduction zones, but what is sampled outboard trenches may have little resemblance to what is contributed to arc volcanoes because of the metamorphic transformations affecting the subducting slab at different P-T gradients (Bebout, 2013; Gómez-Tuena et al., 2011). The residual mineral assemblages at the onset of sediment melting are in turn difficult to predict, but they should be mainly controlled by the initial bulk compositions and the metamorphic pathways along the subduction channel (Spandler and Pirard, 2013; Woodland et al., 2018; Xiao et al., 2013). Because the two sedimentary units sampled outboard Colombia differ significantly in the modal abundance of carbonate versus clay and apatite (see Beiersdorf and Rösch, 1983), their metamorphic and residual mineral assemblages upon melting are also expected to differ. High-pressure melting experiments of carbonate-rich sediments produce granitic liquids in equilibrium with carbonate phases, pyroxene and garnet, but show no significant fraction of residual mica or apatite at temperatures >1000 °C (Skora et al., 2015; Tsuno et al., 2012). In contrast, apatite and mica (biotite or phengite) can both remain stable during melting of carbonate-poor sediments, even at high P-T conditions (Johnson and Plank, 2000; Skora et al., 2015). In accordance to this, we estimate that carbonates and Ca-rich garnets would be more abundant during melting of the meta-sediments from the lower carbonate-rich unit, whereas mica and phosphates would be the likely residual phases during melting of the upper hemipelagic clay-rich unit (see Table 2).

Fig. 9 shows how elemental ratios can be fractionated during partial melting of the different subducted sediments, even up to relatively high melt fractions (~30%). A strong fractionation of the Th/La and Sm/La ratios is predicted by existence of residual apatite, which has a strong partitioning of La over Th, but also of Sm over La ($K_dTh << K_dLa << K_dSm$; Prowatke and Klemme, 2006). Apatite is originally present in the upper hemipelagic sediments with up to ~15% modal abundance in some layers (Beiersdorf and Rösch, 1983). Recent experimental studies have also demonstrated the compatibility of La over Th during carbonate melting (Skora et al., 2015), indicating that the overall higher Th/La ratios observed in the Colombian volcanoes may also be influenced by residual carbonates, which are abundant throughout the sedimentary column. This evidence supports the idea that melting of carbonate-rich trench sediments would transfer higher Th/La ratios to the Colombian and possibly to the Central American arc (see Plank, 2005).

The presence of residual mica like biotite or phengite has commonly been invoked to govern the fractionation of LILE/REE ratios like Rb/La and Ba/La (Hermann and Rubatto, 2009; Johnson and Plank, 2000). The expected variable modal abundance of mica can therefore produce diverging melting pathways than can account for the variable LILE/REE trends in the volcanoes (Fig. 9c and d). The variability of these ratios in arc rocks, however, has also been related to the participation of slab fluids, given the preferentially solubility of Ba and Rb over La (Class et al., 2000; Elliott et al., 1997). Nonetheless, and even though fluids are a ubiquitous phase during subduction (Schmidt and Poli, 2013), melt-controlled ratios (Th/La or Sm/La) positively correlate with Rb/La (Fig. 9c) and Ba/La ratios (not shown) in both NSI and CMV volcanoes, suggesting that the observed differences might in turn be inherited from the incorporation of different sediment melts (see Kelemen et al., 2004). The modeled fractionation trends, although mainly controlled by the abundance of mica, also depend on the initial ratios in both bulk sediments. In Fig. 9d, for example, the divergent trends do not seem to be controlled by the Ba/La ratio, as both volcanic rocks and both bulk sediments display similar values, but instead by the strong differences in the U/La ratios in the sedimentary units and their modeled fractionations upon melting.

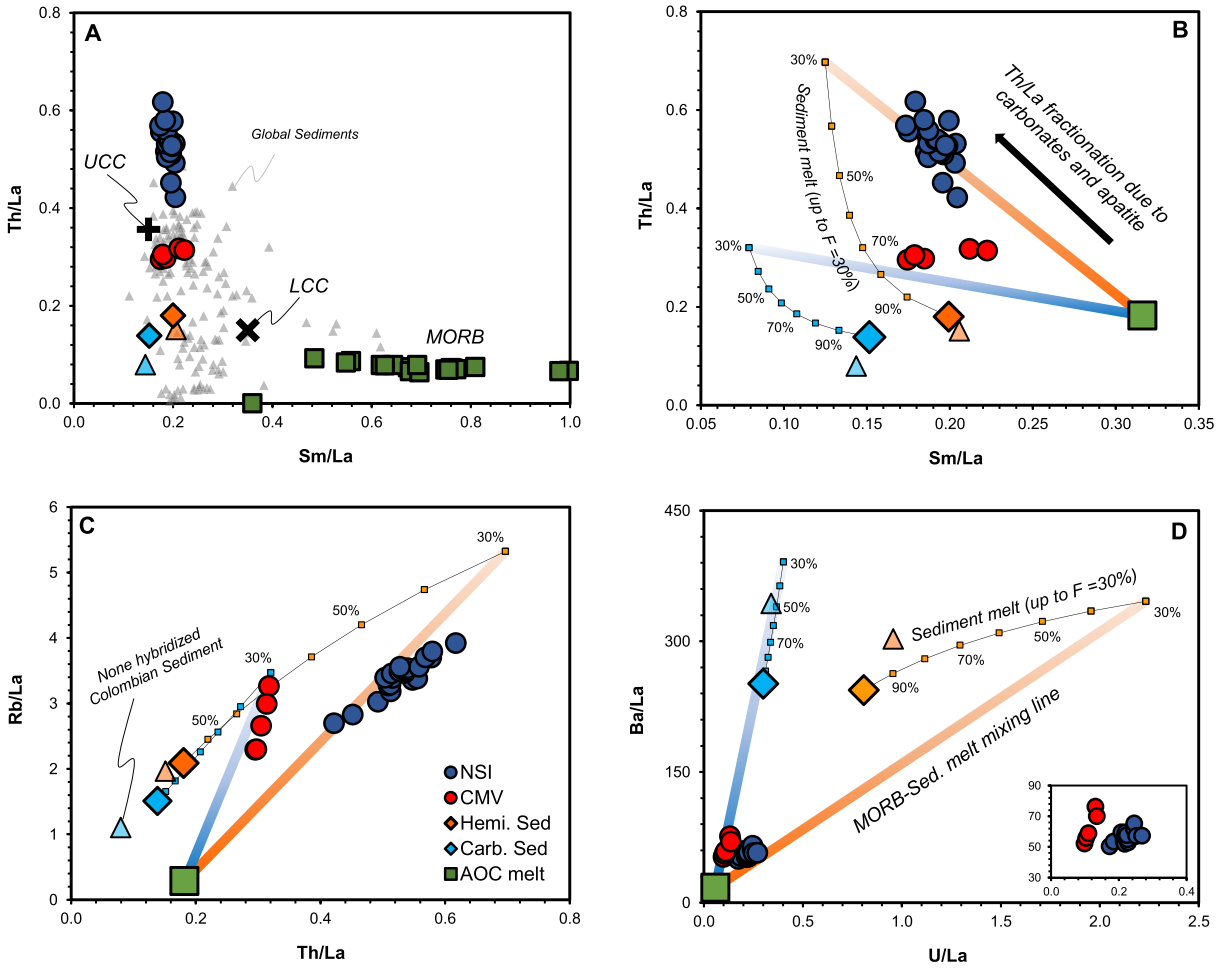

Fig. 9. (A) Sm/La vs. Th/La. NSI rocks display higher Th/La values than those found in the global spectrum of trench sediments (Vervoort et al., 2011) and the Upper Continental Crust (UCC) and Lower Continental Crust (LCC) averages from Rudnick and Fountain (1995). (B, C, D) Geochemical modelling for sediment melting (see Discussion). Sediment melting considering up to 30% of partial melting from bulk hemipelagic and bulk carbonate sediments (see Table 2). AOC melt considering 5% of partial melting of average EPR MORB from Gale et al. (2013). Gradient orange line denotes mixing between AOC melt and hemipelagic sediment partial melt (30% F). Blue gradient line denotes mixing between AOC and carbonate sediment melt mixing for 30% sediment partial melting. Mineralogical constraints for AOC and sediment melting and partition coefficients used for modelling can be found in Table 2. The trace element systematics shows a striking similarity between the different sedimentary packages and the arc volcanoes. Divergent trend lines from NSI and CMV can be explained by mixing between the two contrasting subducted materials. Also shown, non-hybridized Colombian sediment (triangles) from Table 1.

The elemental and residual assemblages predicted for the different sedimentary packages produce unique end-member compositions that can satisfy the mixing relationships displayed by the studied volcanoes when mixed with a depleted MORB-like Altered Oceanic Crust (AOC) melt component (Fig. 9) (see Discussion below). The high Th and U contents and the high Th(U)/La ratios observed in NSI appear to be governed by the incorporation of melts coming from the hemipelagic apatite/clay-rich sedimentary unit (Fig. 9). On the contrary, rocks from CMV appear to be inheriting the low Th and U contents from the lower carbonate-rich sedimentary unit, and their compositions are thus consistent with the incorporation of a carbonate-rich melt with higher Ba/La but lower Th/La and U/La ratios. The geochemical mimicry between the sedimentary units and the studied arc volcanoes let us to conclude that the compositional variability observed in the NVP rocks could be inherited directly from the subducted sedimentary components undergoing partial melting at subarc depths.

6.5. Isotopic constrains in the sedimentary incorporation

Now that there is a hypothesis for the compositional variability of the studied samples, we will test if the contrasting isotopic compositions of the studied volcanoes can be explained by the incorporation of different sedimentary packages that mix with a depleted MORB-like or AOC component (Fig. 10). Firstly, the isotopic variability of the studied volcanoes allows to differentiate the role of the subducted oceanic plate and constrain the nature of the depleted component. The volcanic rocks display tight linear correlations in $^{208}Pb/^{204}Pb$ vs. Sr/Pb (Fig. 10a) ratios that depart from the compositions of the sediment melts and extend towards an isotopically depleted end-member with a higher Sr/Pb ratio than the mantle or the Nazca plate MORB (see Fig. 10a). Since Pb is considered to be more soluble than Sr during dehydration of an AOC, and both elements behave similarly incompatible during MORB melting at high pressures (Kessel et al., 2005), we suggest that the depleted component is incorporated in the form of a melt coming from the subducted AOC. The participation of an AOC melt is also supported by the Sr-Nd isotopic correlation (see Fig. 10d) in which the more depleted samples appear to plot towards the radiogenic Sr values that are typical of this component.

The subtle but discernible decoupling of the Nd-Hf isotopes towards the "seawater array" strongly suggests that marine pelagic sediments like the ones sampled outboard Colombia should be involved in the petrogenesis (Fig. 10b). And yet, Pacific sediments display Hf and Pb isotope compositions that are inadequate mixing end-members for the studied volcanoes. As mentioned before, we suggest that the Colombian trench sediments had a small contribution from an Atlantic-like sedimentary source that shifted the Hf and Pb isotopic

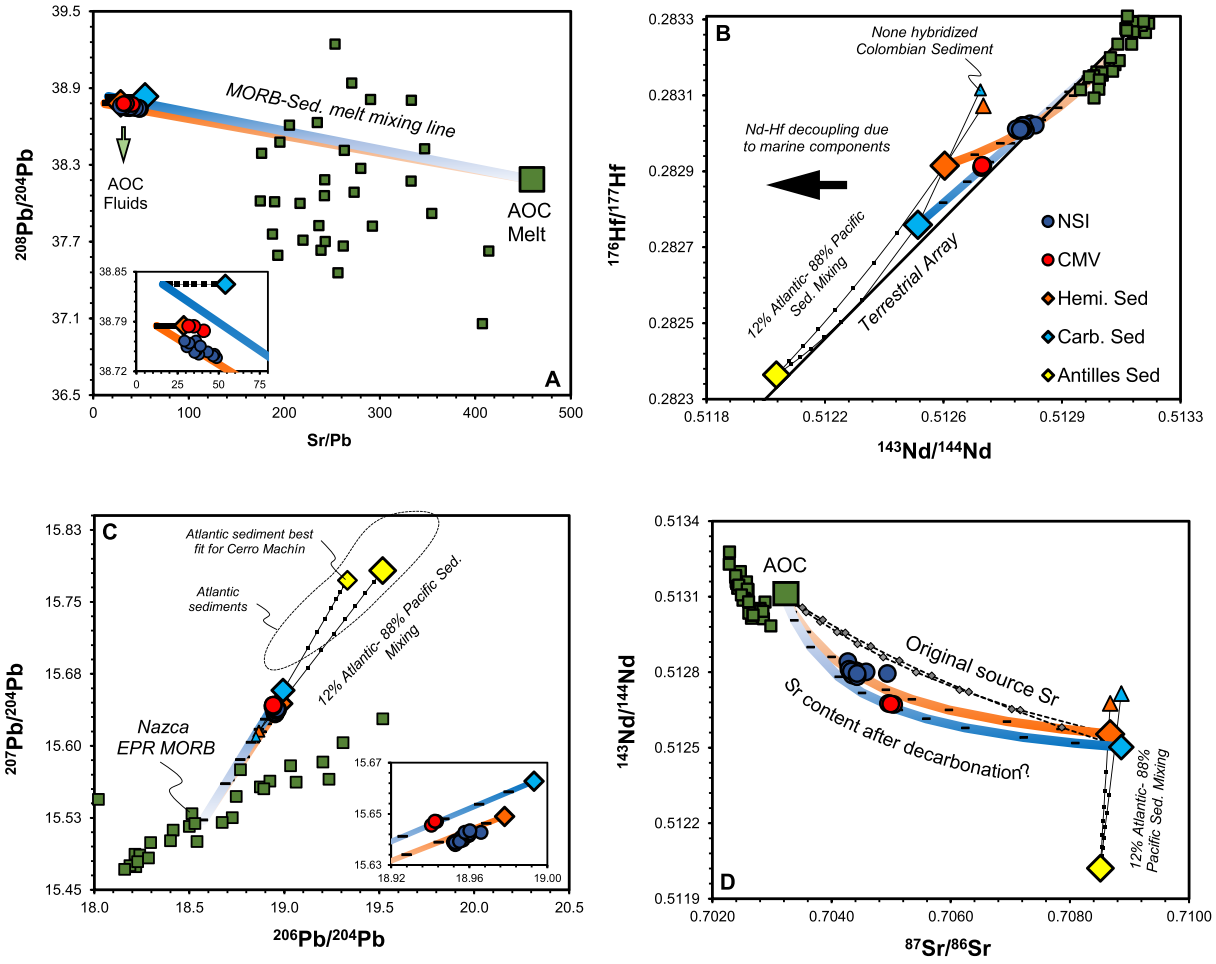

Fig. 10. Isotopic and trace element systematics of rocks from the studied area. (A) Sr/Pb vs. $^{208}Pb/^{204}Pb$. NVP rocks plots towards an AOC melt component with higher Sr/Pb ratios than MORB. (B, C) Nd-Hf and Pb-Pb mixing between an AOC melt component and the different subducted sedimentary packages. Mixing lines account for the observed isotopic composition for the studied rocks. (D) Sr-Nd isotopic composition and mixing between AOC and the sedimentary packages. Hyperbolic mixing lines considering up to 75% Sr loss during decarbonation. Mixing lines with original Sr contents in the sediments are also shown.

compositions while leaving the Nd and Sr isotopes almost unchanged (Fig. 10). By using these hybridized sediments in Nd-Hf-Pb isotopic space (Fig. 10b and c), and in accordance with the trace-element constraints discussed above, the isotopic compositions of NSI can be reproduced by the incorporation of the hemipelagic sediment, whereas CMV seems governed by the carbonate-rich sedimentary layer.

An interesting situation arises, however, when the Sr-Nd isotopic systems are more carefully observed (Fig. 10d). Nielsen and Marschall (2017) recently suggested that, on a global scale, the Sr-Nd isotopic variations displayed by arc rocks can be explained by mixing a mantle peridotite with MORB-like isotopes with their corresponding trench sediments. Nonetheless, this is only true when the sedimentary component has lower Sr/Nd ratios than the isotopically depleted MORB-like component. For example, while the Sr/Nd ratio of a typical mantle peridotite is around 13 (Workman and Hart, 2005) and ~11 for a normal MORB (Gale et al., 2013), the Sr/Nd ratios of the hemipelagic and carbonate units outboard Colombia are ~50 and ~112, respectively. These values are too high for constructing any satisfactory hyperbolic mixing curve for the studied volcanoes (see Fig. 10d). The sedimentary Sr/Nd ratio cannot be significantly modified by melting because Sr and Nd have similar compatibility during melting of carbonate-rich sediments (Skora et al., 2015). Another possibility would be to increase the Sr/Nd ratio of the depleted component by invoking fluids or melts from the subducted AOC, but not even a low extent partial melt (5%) of a Sr-rich AOC appears sufficient to reproduce the hyperbolic mixing trend of the Colombian volcanoes.

A possible solution to this problem could be related to the soluble behavior of Sr during decarbonation, a process that is expected to occur during subduction of sedimentary carbonates (Kerrick and Connelly, 2001; Poli, 2015). Decarbonation occurs when CO_2 rich fluids are released from the subducted materials along the subduction pathway. These liberated fluids could also carry other mobile species like Sr, which is a major constituent of the carbonate phase. Interestingly, decarbonation does not appear to mobilize other fluid-mobile elements like Pb, because it is probably hosted in less-soluble detrital minerals like zircon or apatite. Since the Nd-Pb-Hf isotopic composition of the volcanic rocks can be successfully reproduced by the mixing models, and only Sr appears offset, we suggest that up to ~75% of the initial Sr was lost from the sediments by decarbonation before reaching the melting region below the volcanoes. It is important to note, however, that volcanoes from the North Andean Zone, and especially Nevado del Ruiz volcano, releases some of the highest quantities of magmatic CO_2 in the world (Aiuppa et al., 2017), suggesting that not all subducted carbonate is lost during decarbonation and that an important portion is being transferred back to the atmosphere by the erupting volcanoes.

6.6. Insights into the origin of the NVP

The geochemical evidence discussed above indicates that the source regions of the studied volcanoes are not only different in terms of their isotopic and trace element compositions, but that the P-T conditions under which melting occurred must also differ (Fig. 7). The stability of

amphibole in subducted lithologies is limited to 70–90 km deep (Allen and Boettcher, 1983; Davies and Stevenson, 1992), and amphibole is therefore unstable at the projected slab depth of 140–160 km below the volcanoes. At those depths, a nearly anhydrous eclogite would be the most likely metamorphic facies in any kind of subducted lithology (Poli and Schmidt, 2002). While rocks from CMV do indeed have the fractionated REE patterns and Nb/Ta ratios that signal melting of deep eclogites, inferring an "adakitic" origin related to melting of a subducted MORB (Defant and Drummond, 1990) is not supported because of their enriched isotopic compositions. The REE and Nb/Ta ratios of NSI point to the presence of residual amphibole instead, even if the crustal and slab parameters are not significantly different from those of CMV. Consequently, a possible scenario to explain the pressure dependent mineralogical residual assemblage for both NSI and CVM might be related to pressure-dependent fractionations occurring in the mantle domain and not directly at the slab surface.

Recent studies have shown that subducted crustal lithologies like sediments and eroded forearc debris behave buoyantly in the subduction channel, even if buried to ultra-high-pressure conditions (Behn et al., 2011; Hacker et al., 2011). Numerical simulations have also shown that subduction mélanges —constituted by heterogeneous mixture of subducted lithologies in a schistose matrix of hydrous minerals— can be diapirically exhumed into the mantle wedge where they can undergo extensive melting (Castro et al., 2013; Gerya, 2011). It has been recently proposed that mélanges like these can generate high-Mg# andesites upon partial melting directly in the mantle wedge without the intervention of parental basalts (Gómez-Tuena et al., 2016; Gómez-Tuena et al., 2018; Parolari et al., 2018). In the light of this, we suggest that the origin of the NVP andesites might be governed by melting of sediment-rich diapirs that detached from the subducted slab and were incorporated in the mantle wedge at different depths (Fig. 11). Andesitic magmas of NSI could be formed by melting of a slab diapir that contained a higher proportion hemipelagic sediments at pressures below the stability of amphibole (Ionov and Hofmann, 1995). Conversely, the diapir that formed CMV had a larger proportion of carbonate and melted at a greater depth, thus enhancing the stability of garnet and rutile in the residue. The specific pathway followed by subducted materials within the mantle wedge can therefore enhance the reworking of refractory carbonate lithologies, as these sedimentary components enter to the hot corner of the overlying mantle wedge (Kelemen and Manning, 2015). We suggest that the differences in slab depth below the volcanoes, and the fact that the lower carbonate-rich layer might be the last to be detached from slab, had a direct influence in the sedimentary components being incorporated into each volcano (see Fig. 11).

6.7. North Andean xenoliths as evidence from subduction mélanges?

The isotopic similarities between the lower crustal and mantle xenoliths from the SVP (Weber, 1998; Weber et al., 2002) and the arc rocks of the Northern Colombian Andes might indeed indicate a co-genetic origin, albeit not one related to crustal contamination of the ascending magmas as previously considered (Marín-Cerón et al., 2010). Recent studies on some mantle clinopyroxenite xenoliths, showing the petrologic signatures of reaction between peridotite and silicic melts or fluids, have established equilibration pressures of up to ~150 km depth using garnet and pyroxene thermobarometry with average errors of no more than 0.1 GPa (~3.6 km) (Bloch et al., 2017; Weber et al., 2002). These studies have also shown that the age of some clinopyroxenites can be as young as 5 Ma, thus disregarding the possibility that these xenoliths represent relicts of an ancient lower crust below the Colombian Central Cordillera (Bloch et al., 2017). More importantly, however, is that their isotopic compositions, and especially their radiogenic Pb, must then represent deep mantle features, the origin of which could be intimately linked to the slab-derived metasomatic agents involved in the petrogenesis of arc magmas. Interestingly, some of these xenoliths are carbonated-bearing pyroxenites and peridotites that exhibit Ca-rich phases such as aragonite, dolomite and Mg-calcite (Ferri et al., 2017; Weber, 1998), indeed arguing for important deep carbon fluxes into the North Andean mantle related to the unique sedimentary carbonated sequences at the trench.

The xenoliths may very well be fragments of a foundering lithosphere (Bloch et al., 2017), but it is also possible that they could represent the unmolten dense remnants of the rising diapirs that gave birth to the arc volcanoes. In this case, melts derived from slab diapirs might migrate upwards to feed shallow magmatic reservoirs and eventually erupt, while residual mélange lithologies would likely "relaminate" at the base of the lithosphere (Kelemen and Behn, 2016) forming the currently unstable crustal roots of the Colombian Northern

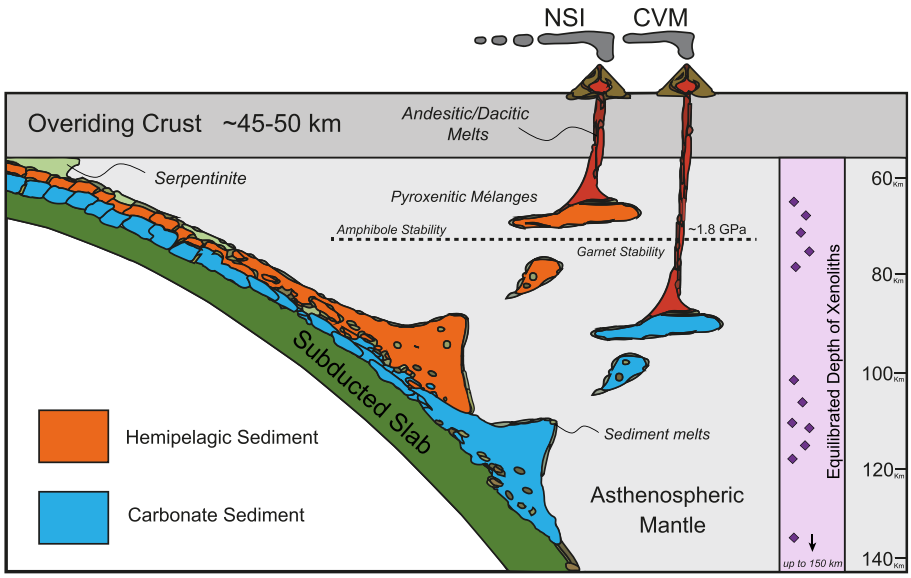

Fig. 11. Schematic diagram for the formation of NVP rocks. Sedimentary packages are introduced to the mantle in the form of buoyant diapirs that undergo melting at different depths. Melt fractionation for NSI occurs under the amphibole stability field, while the CVM is formed by garnet and rutile fractionation at deeper conditions. Stability fields according to Davies and Stevenson (1992) and Allen and Boettcher (1983). Pressure calculations for mantle and crustal xenoliths are also shown (Bloch et al., 2017; Weber et al., 2002). Cartoon model modified from Nielsen and Marschall (2017).

Andes. In other words, volcanoes and xenoliths could be complements of one single system that is intimately linked to the Colombian subduction zone (Fig. 11).

7. Concluding remarks

The geochemical evidence presented above, when visualized in terms of the local tectonic context, suggests that Quaternary volcanism in the northernmost Andean chain is controlled by melting of two compositionally contrasting subducted sediments that were incorporated into the mantle wedge as buoyant diapirs. The specific pathways followed by these diapirs are still not clear, but at least for the Colombian Northern Andes, there is a strong indication that they might undergo melting at different depths, shown by the REE and Nb/Ta variations of the volcanic products. The incorporation of bulk sediments into subduction mélanges might explain the compositional characteristics of some arc sections (Nielsen and Marschall, 2017; Parolari et al., 2018; Plank, 2005), but in the case of the Colombian margin, where refractory carbonates are being subducted, there appears to be strong element fractionation during melting of the subducted sedimentary components, as evidenced by the unusually high Th/La ratios of the arc products.

The studied volcanoes exhibit enriched Pb and Hf compositions that cannot be reconciled with the incorporation of any crustal or sedimentary component within the current geotectonic makeup of the Northern Andes. In turn, the isotopic compositions of the NVP suggest the participation of an Atlantic-like sediment that most likely polluted or hybridized the subducted sedimentary sequence under an open Central American Seaway. Nonetheless, volcanoes from the NVP display Nd-Hf isotopic decoupling that is also in agreement with the incorporation of a Pacific-like carbonate-rich pelagic sediment.

Regardless of the specific process of sedimentary hybridization, North Andean xenoliths that possibly formed by reaction of silicic melts from the down going slab (Bloch et al., 2017) yield enriched Pb isotopic composition and carbonated-bearing assemblages that reinforce our interpretation of subduction-related metasomatic agents. The most important feature of these xenoliths, however, is that they show a remarkable isotopic resemblance with the arc rocks that erupt along the Colombian Northern Andes and thus make them a potential analog for mantle remnants of subducted mélange lithologies. The connection between these xenoliths and the sedimentary signatures from the volcanic rocks further supports an increasingly recognized hypothesis: continental intermediate arc magmatism can be derived from melting of the subducted-modified mantle wedge.

Acknowledgments

We are grateful to Liliana Corona, Ofelia Pérez, Carlos Ortega, Manuel Albarrán and Wilton Echavarría for their help during sample preparation and analysis. We highly appreciate the help of Nicolás Estrada, Carlos Andrés Jimenez and Mauricio Sierra for their enduring performance in the Colombian highlands during fieldwork. Productive discussions with Mattia Parolari were helpful in the development of this research. We thank the International Ocean Discovery Program Gulf Coast Repository (Texas, USA) for suppling the analyzed offshore DSDP samples. The manuscript benefited greatly from the thoughtful suggestions of two anonymous reviewers. Editorial handling by Andrew Kerr is highly appreciated. This work was supported by undergraduate scholarships granted by the Laboratorio de Estudios Isotópicos (LEI) of the Centro de Geociencias, UNAM and by the Departamento de Investigación of Universidad EAFIT, Colombia.

Appendix A, B, and C. Supplementary data

Supplementary data to this article can be found online at https://doi.org/10.1016/j.lithos.2019.04.007.

References

Aiuppa, A., Fischer, T.P., Plank, T., Robidoux, P., Di Napoli, R., 2017. Along-arc, inter-arc and arc-to-arc variations in volcanic gas CO2/ST ratios reveal dual source of carbon in arc volcanism. Earth Sci. Rev. 168, 24–47. https://doi.org/10.1016/j.earscirev.2017.03.005.

Albarède, F., Simonetti, A., Vervoort, J.D., Blichert-Toft, J., Abouchami, W., 1998. A Hf-Nd isotopic correlation in ferromanganese nodules. Geophys. Res. Lett. 25, 3895–3898. https://doi.org/10.1029/1998GL900008.

Allen, J.C., Boettcher, A.L., 1983. The stability of amphibole in andesite and basalt at high pressures. Am. Mineral. 68, 307–314. https://doi.org/scopus/2-s2.0-0020558282.

Alonso-Perez, R., Müntener, O., Ulmer, P., 2009. Igneous garnet and amphibole fractionation in the roots of island arcs: experimental constraints on andesitic liquids. Contrib. Mineral. Petrol. 157, 541–558. https://doi.org/10.1007/s00410-008-0351-8.

Ancellin, M.A., Samaniego, P., Vlastélic, I., Nauret, F., Gannoun, A., Hidalgo, S., 2017. Across-arc versus along-arc Sr-Nd-Pb isotope variations in the Ecuadorian volcanic arc. Geochem. Geophys. Geosyst. 18, 1163–1188. https://doi.org/10.1002/2016GC006679.

Annen, C., Blundy, J.D., Sparks, R.S.J., 2006. The genesis of intermediate and silicic magmas in deep crustal hot zones. J. Petrol. 47, 505–539. https://doi.org/10.1093/petrology/egi084.

Bacon, C.D., Silvestro, D., Jaramillo, C., Smith, B.T., Chakrabarty, P., Antonelli, A., 2015. Biological evidence supports an early and complex emergence of the Isthmus of Panama. Proc. Natl. Acad. Sci. 112, 6110–6115. https://doi.org/10.1073/pnas.1423853112.

Bebout, G.E., 2013. Chemical and isotopic cycling in subduction zones. Treatise on Geochemistry, 2nd ed. Elsevier, pp. 703–747 https://doi.org/10.1016/B978-0-08-095975-7.00322-3.

Behn, M.D., Kelemen, P.B., Hirth, G., Hacker, B.R., Massonne, H.J., 2011. Diapirs as the source of the sediment signature in arc lavas. Nat. Geosci. 4, 641–646. https://doi.org/10.1038/ngeo1214.

Beiersdorf, H., Natland, J.H., 1983. Sedimentary and diagenetic processes in the Central Panama Basin since the Late Miocene: the lithology and composition of sediments from deep sea drilling project sites 504 and 505.

Beiersdorf, H., Rösch, H., 1983. Mineralogy of sediments encountered during deep sea drilling project leg 69 (Costa Rica Rift, Panama Basin), as determined by x-ray diffraction.

Bezard, R., Davidson, J.P., Turner, S., Macpherson, C.G., Lindsay, J.M., Boyce, A.J., 2014. Assimilation of sediments embedded in the oceanic arc crust: myth or reality? Earth Planet. Sci. Lett. 395, 51–60. https://doi.org/10.1016/J.EPSL.2014.03.038.

Bloch, E., Ibañez-Mejia, M., Murray, K., Vervoort, J., Müntener, O., 2017. Recent crustal foundering in the Northern Volcanic Zone of the Andean arc: petrological insights from the roots of a modern subduction zone. Earth Planet. Sci. Lett. 476, 47–58. https://doi.org/10.1016/j.epsl.2017.07.041.

Borrero, C., Toro, L.M., Alvarán, M., Castilllo, 2009. Geochemistry and Tectonic controls of the effusive activity related with Ancentral Nevado del Ruiz volcano, Colombia. Geofis. Int. 48, 149–169.

Bottazzi, P., Tiepolo, M., Vannucci, R., Zanetti, A., Brumm, R., Foley, S.F., Oberti, R., 1999. Distinct site preferences for heavy and light REE in amphibole and the prediction of (Amph/L)D(REE). Contrib. Mineral. Petrol. 137, 36–45. https://doi.org/10.1007/s004100050580.

Carpentier, M., Chauvel, C., Maury, R.C., Mattielli, N., 2009. The "zircon effect" as recorded by the chemical and Hf isotopic compositions of Lesser Antilles forearc sediments. Earth Planet. Sci. Lett. 287, 86–99. https://doi.org/10.1016/j.epsl.2009.07.043.

Castro, A., Vogt, K., Gerya, T., 2013. Generation of new continental crust by sublithospheric silicic-magma relamination in arcs: a test of Taylor's andesite model. Gondwana Res. 23, 1554–1566. https://doi.org/10.1016/j.gr.2012.07.004.

Chiarabba, C., De Gori, P., Faccenna, C., Speranza, F., Seccia, D., Dionicio, V., Prieto, G.A., 2016. Subduction system and flat slab beneath the Eastern Cordillera of Colombia. Geochem. Geophys. Geosyst. 17, 16–27. https://doi.org/10.1002/2015GC006048.

Chiaradia, M., 2015. Crustal thickness control on Sr/Y signatures of recent arc magmas: an Earth scale perspective. Sci. Rep. 5, 8115. https://doi.org/10.1038/srep08115.

Chiaradia, M., Fontbote, L., 2002. Lead isotope systematics of late Cretaceous–Tertiary Andean arc magmas and associated ores between 8 N and 40 S: evidence for latitudinal mantle heterogeneity. Terra Nova 14, 337–342.

Class, C., Miller, D.M., Goldstein, S.L., Langmuir, C.H., 2000. Distinguishing melt and fluid subduction components in Umnak Volcanics, Aleutian Arc. Geochem. Geophys. Geosyst. 1. https://doi.org/10.1029/1999GC000010 (n/a-n/a).

Clift, P., Schouten, H., Vannucchi, P., 2009. Arc–continent collisions, sediment recycling and the maintenance of the continental crust. Earth Accretionary Syst. Space Time, 75–103 https://doi.org/10.1144/SP318.3.

Cochrane, R., Spikings, R., Gerdes, A., Winkler, W., Ulianov, A., Mora, A., Chiaradia, M., 2014. Distinguishing between in-situ and accretionary growth of continents along active margins. Lithos 202–203, 382–394. https://doi.org/10.1016/j.lithos.2014.05.031.

Davidson, J., Turner, S., Handley, H., Macpherson, C., Dosseto, A., 2007. Amphibole "sponge" in arc crust? Geology 35, 787–790. https://doi.org/10.1130/G23637A.1.

Davies, J.H., Stevenson, D.J., 1992. Physical model of source region of subduction zones volcanics. J. Geophys. Res. 97, 2037–2070.

Defant, M.J., Drummond, M.S., 1990. Derivation of some modern arc magmas by melting of young subducted lithosphere. Nature 347, 662–665. https://doi.org/10.1038/347662a0.

Elliott, T., Plank, T., Zindler, A., White, W., Bourdon, B., 1997. Element transport from slab to volcanic front at the Mariana arc. J. Geophys. Res. Solid Earth 102, 14991–15019. https://doi.org/10.1029/97JB00788.

Ferri, F., Poli, S., Rodríguez-Vargas, A., 2017. Andean volcanoes record carbonatite mantle metasomatism and CO2 degassing at subduction zones. Goldschmidt2017 (Abstract 05b, 2157).

Gale, A., Dalton, C.A., Langmuir, C.H., Su, Y., Schilling, J.G., 2013. The mean composition of ocean ridge basalts. Geochem. Geophys. Geosyst. 14, 489–518. https://doi.org/10.1029/2012GC004334.
Gerya, T., 2011. Future directions in subduction modeling. J. Geodyn. 52, 344–378. https://doi.org/10.1016/j.jog.2011.06.005.
Gill, J.B., 1981. Orogenic andesites and plate tectonics, orogenic andesites and plate tectonics. https://doi.org/10.1007/978-3-642-68012-0.
Gómez-Tuena, A., Mori, L., Goldstein, S.L., Pérez-Arvizu, O., 2011. Magmatic diversity of western Mexico as a function of metamorphic transformations in the subducted oceanic plate. Geochim. Cosmochim. Acta 75, 213–241. https://doi.org/10.1016/j.gca.2010.09.029.
Gómez-Tuena, A., Straub, S.M., Zellmer, G.F., 2014a. An introduction to orogenic andesites and crustal growth. Geol. Soc. Lond. Spec. Publ. 385, 1–13. https://doi.org/10.1144/sp385.16.
Gómez-Tuena, A., Díaz-Bravo, B., Vázquez-Duarte, A., Pérez-Arvizu, O., Mori, L., 2014b. Andesite petrogenesis by slab-derived plume pollution of a continental rift. Geol. Soc. Lond. Spec. Publ. 385, 65–101. https://doi.org/10.1144/SP385.4.
Gómez-Tuena, A., Mori, L., Straub, S.M., 2016. Geochemical and petrological insights into the tectonic origin of the Transmexican Volcanic Belt. Earth Sci. Rev. https://doi.org/10.1016/j.earscirev.2016.12.006.
Gómez-Tuena, A., Cavazos-Tovar, J.G., Parolari, M., Straub, S.M., Espinasa-Pereña, R., 2018. Geochronological and geochemical evidence of continental crust 'relamination' in the origin of intermediate arc magmas. Lithos 322, 52–66. https://doi.org/10.1016/j.lithos.2018.10.005.
Goss, A.R., Kay, S.M., 2006. Steep REE patterns and enriched Pb isotopes in southern Central American arc magmas: evidence for forearc subduction erosion? Geochem. Geophys. Geosyst. 7. https://doi.org/10.1029/2005GC001163.
Green, T., 1995. Significance of ? As an indicator of geochemical processes in the crust-mantle system. Chem. Geol. 120, 347–359. https://doi.org/10.1016/0009-2541(94)00145-X.
Gutscher, M.A., Malavieille, J., Lallemand, S., Collot, J.Y., 1999. Tectonic segmentation of the North Andean margin: impact of the Carnegie Ridge collision. Earth Planet. Sci. Lett. 168, 255–270. https://doi.org/10.1016/S0012-821X(99)00060-6.
Hacker, B.R., Kelemen, P.B., Behn, M.D., 2011. Differentiation of the continental crust by relamination. Earth Planet. Sci. Lett. 307, 501–516. https://doi.org/10.1016/j.epsl.2011.05.024.
Hart, S.R., Dunn, T., 1993. Experimental cpx/melt partitioning of 24 trace elements. Contrib. Mineral. Petrol. 113, 1–8. https://doi.org/10.1007/BF00320827.
Hawkesworth, C.J., Turner, S.P., McDermott, F., Peate, D.W., Van Calsteren, P., 1997. U-Th isotopes in arc magmas: implications for element transfer from the subducted crust. Science 276, 551–555. https://doi.org/10.1126/science.276.5312.551.
Hayes, G.P., Wald, D.J., Johnson, R.L., 2012. Slab1.0: a three-dimensional model of global subduction zone geometries. J. Geophys. Res. Solid Earth 117, 1–15. https://doi.org/10.1029/2011JB008524.
Hermann, J., Rubatto, D., 2009. Accessory phase control on the trace element signature of sediment melts in subduction zones. Chem. Geol. 265, 512–526. https://doi.org/10.1016/j.chemgeo.2009.05.018.
Hildreth, W., Moorbath, S., 1988. Crustal contribution to arc magmatism in the Andes of Central Chile. Contrib. Mineral. Petrol. 98, 455–489. https://doi.org/10.1007/BF00372365.
Ionov, D.A., Hofmann, A.W., 1995. Nb Ta-rich mantle amphiboles and micas: implications for subduction-related metasomatic trace element fractionations. Earth Planet. Sci. Lett. 131, 341–356. https://doi.org/10.1016/0012-821X(95)00037-D.
James, D.E., Murcia, L.A., 1984. Crustal contamination in northern Andean volcanics. J. Geol. Soc. Lond. 141, 823–830. https://doi.org/10.1144/gsjgs.141.5.0823.
Jiang, S., Wise, S.W., Wang, Y., 2007. Chapter4. Cause of the Middle/Late Miocene Carbonate Crash : Dissolution or Low Productivity? Proceedings of the Ocean Drilling Program, Scientific Results 206 https://doi.org/10.2973/odp.proc.sr.206.013.2007.
Johnson, K.T.M., 1994. Experimental cpx/ and garnet/melt partitioning of REE and other trace elements at high pressures: petrogenetic implications. Mineral. Mag. 58A, 454–455. https://doi.org/10.1180/minmag.1994.58A.1.236.
Johnson, M.C., Plank, T., 2000. Dehydration and melting experiments constrain the fate of subducted sediments. Geochem. Geophys. Geosyst. 1. https://doi.org/10.1029/1999GC000014.
Kelemen, P.B., 1995. Genesis of high Mg# andesites and the continental crust. Contrib. Mineral. Petrol. 120, 1–19. https://doi.org/10.1007/BF00311004.
Kelemen, P.B., Behn, M.D., 2016. Formation of lower continental crust by relamination of buoyant arc lavas and plutons. Nat. Geosci. https://doi.org/10.1038/ngeo2662.
Kelemen, P.B., Manning, C.E., 2015. Reevaluating carbon fluxes in subduction zones, what goes down, mostly comes up. Proc. Natl. Acad. Sci. 112, E3997–E4006. https://doi.org/10.1073/pnas.1507889112.
Kelemen, P.B., Hanghøj, K., Greene, A.R., 2003. One view of the geochemistry of subduction-related magmatic arcs, with an emphasis on primitive andesite and lower crust. Treatise on Geochemistry, 2nd ed. vol. 4, pp. 749–806. https://doi.org/10.1016/B978-0-08-095975-7.00323-5.
Kelemen, P.B., Yogodzinski, G.M., Scholl, D.W., 2004. Along-strike variation in the aleutian island arc: Genesis of high Mg# andesite and implications for continental crust. Geophysical Monograph Series. American Geophysical Union (AGU), pp. 223–276 https://doi.org/10.1029/138GM11.
Kelley, K.A., Plank, T., Farr, L., Ludden, J., Staudigel, H., 2005. Subduction cycling of U, Th, and Pb. Earth Planet. Sci. Lett. 234, 369–383. https://doi.org/10.1016/j.epsl.2005.03.005.
Kerr, A.C., Marriner, G.F., Tarney, J., Nivia, A., Saunders, A.D., Thirlwall, M.F., Sinton, C.W., 1997. Cretaceous basaltic terranes in Western Colombia: elemental, chronological and Sr-Nd isotopic constraints on petrogenesis. J. Petrol. 38, 677–702. https://doi.org/10.1093/petroj/38.6.677.
Kerrick, D.M., Connelly, J.A.D., 2001. Metamorphic devolatilization of subducted marine sediments and the transport of volatiles into the Earth's mantle. Nature 411, 293–296. https://doi.org/10.1038/35077056.
Kessel, R., Schmidt, M.W., Ulmer, P., Pettke, T., 2005. Trace element signature of subduction-zone fluids, melts and supercritical liquids at 120–180 km depth. Nature 437, 724–727. https://doi.org/10.1038/nature03971.
Laeger, K., Halama, R., Hansteen, T., Savov, I.P., Murcia, H.F., Cortés, G.P., Garbe-Schönberg, D., 2013. Crystallization conditions and petrogenesis of the lava dome from the ~900yearsBP eruption of Cerro Machín Volcano, Colombia. J. S. Am. Earth Sci. 48, 193–208. https://doi.org/10.1016/j.jsames.2013.09.009.
Le Maitre, R.W., Streckeisen, A., Zanettin, B., Le Bas, M.J., Bonin, B., Bateman, P. (Eds.), 2002. Igneous Rocks. Cambridge University Press, Cambridge https://doi.org/10.1017/CBO9780511535581.
Lonsdale, P., 2005. Creation of the Cocos and Nazca plates by fission of the Farallon plate. Tectonophysics 404, 237–264. https://doi.org/10.1016/J.TECTO.2005.05.011.
Lyle, M., Dadey, K.A., Farrell, J.W., 1995. The Late Miocene (11-8 Ma) Eastern Pacific Carbonate Crash: evidence for reorganization of deep-water circulation by the closure of the Panama Gateway. Proceedings of the Ocean Drilling Program, pp. 821–838 https://doi.org/10.2973/odp.proc.sr.138.157.1995 138 Scientific results 138.
Macdonald, G.A., Katsura, T., 1964. Chemical composition of Hawaiian lavas. J. Petrol. 5, 82–133. https://doi.org/10.1093/petrology/5.1.82.
Marín-Cerón, M.I., Moriguti, T., Makishima, A., Nakamura, E., 2010. Slab decarbonation and CO2 recycling in the Southwestern Colombian volcanic arc. Geochim. Cosmochim. Acta 74, 1104–1121. https://doi.org/10.1016/j.gca.2009.10.031.
Martínez, L.M., Pulgarin-Alzate, B.A., Sofia, N.A., Correa, A.M., Murcia, H.F., Rueda, J.B., Zuluaga, I., Valencia, L.G., Ceballos Hernández, J.A., Narváez, B.L., Pardo-Villaveces, N., 2014. Geología y Estratigrafía del Complejo Volcánico Nevado del Ruíz.
Molnar, P., 2008. Closing of the central American Seaway and the ice age: a critical review. Paleoceanography 23, 1–15. https://doi.org/10.1029/2007PA001574.
Mori, L., Gómez-Tuena, A., Cai, Y., Goldstein, S.L., 2007. Effects of prolonged flat subduction on the Miocene magmatic record of the central Trans-Mexican Volcanic Belt. Chem. Geol. 244, 452–473. https://doi.org/10.1016/j.chemgeo.2007.07.002.
Nauret, F., Samaniego, P., Ancellin, M.A., Tournigand, P.Y., Le Pennec, J.L., Vlastelic, I., Gannoun, A., Hidalgo, S., Schiano, P., 2018. The genetic relationship between andesites and dacites at Tungurahua volcano, Ecuador. J. Volcanol. Geotherm. Res. 349, 283–297. https://doi.org/10.1016/j.jvolgeores.2017.11.012.
Nielsen, S.G., Marschall, H.R., 2017. Geochemical evidence for mélange melting in global arcs. Sci. Adv. 3, 1–7. https://doi.org/10.1126/sciadv.1602402.
Nof, D., Van Gorder, S., 2003. Did an open Panama Isthmus correspond to an invasion of Pacific water into the Atlantic? J. Phys. Oceanogr. 33, 1324–1336. https://doi.org/10.1175/1520-0485(2003)033<1324:DAOPIC>2.0.CO;2.
Parolari, M., Gómez-Tuena, A., Cavazos-Tovar, J.G., Hernández-Quevedo, G., 2018. A balancing act of crust creation and destruction along the western Mexican convergent margin. Geology 46, 455–458. https://doi.org/10.1130/G39972.1.
Patino, L.C., Carr, M.J., Feigenson, M.D., 2000. Local and regional variations in central American arc lavas controlled by variations in subducted sediment input. Contrib. Mineral. Petrol. 138, 265–283. https://doi.org/10.1007/s004100050562.
Peccerillo, A., Taylor, S.R., 1976. Geochemistry of eocene calc-alkaline volcanic rocks from the Kastamonu area, Northern Turkey. Contrib. Mineral. Petrol. 58, 63–81. https://doi.org/10.1007/BF00384745.
Piedrahita, D.A., Aguilar-Casallas, C., Arango-Palacio, E., Murcia, H., 2018. Estratigrafía del cráter y morfología del volcán Cerro Machín, Colombia. Boletín de Geología 40, 29–48. https://doi.org/10.18273/revbol.v40n3-2018002.
Pindell, J.L., Kennan, L., 2009. Tectonic evolution of the Gulf of Mexico, Caribbean and northern South America in the mantle reference frame. The Geology and Evolution of the Region between North and South America, pp. 1–55.
Plank, T., 2005. Constraints from Thorium/Lanthanum on sediment recycling at subduction zones and the evolution of the continents. J. Petrol. 46, 921–944. https://doi.org/10.1093/petrology/egi005.
Plank, T., 2013. The chemical composition of subducting sediments. Treatise on Geochemistry, 2nd ed. Elsevier Ltd https://doi.org/10.1016/B978-0-08-095975-7.00319-3.
Plank, T., Langmuir, C.H., 1993. Tracing trace elements from sediment input to volcanic output at subduction zones. Nature 362, 739–743. https://doi.org/10.1038/362739a0.
Plank, T., Langmuir, C.H., 1998. The chemical composition of subducting sediment and its consequences for the crust and mantle. Chem. Geol. 145, 325–394. https://doi.org/10.1016/S0009-2541(97)00150-2.
Plank, T., Balzer, V., Carr, M., 2002. Nicaraguan volcanoes record paleoceanographic changes accompanying closure of the Panama gateway. Geology 30, 1087–1090. https://doi.org/10.1130/0091-7613(2002)030<1087:NVRPCA>2.0.CO;2.
Poli, S., 2015. Carbon mobilized at shallow depths in subduction zones by carbonatitic liquids. Nat. Geosci. 8, 633–636. https://doi.org/10.1038/ngeo2464.
Poli, S., Schmidt, M.W., 2002. Petrology of subducted slabs. Annu. Rev. Earth Planet. Sci. 30, 207–235. https://doi.org/10.1146/annurev.earth.30.091201.140550.
Poveda, E., Monsalve, G., Vargas, C., 2015. Receiver functions and crustal structure of the northwestern Andean region, Colombia. J. Geophys. Res., 2408–2425 https://doi.org/10.1002/2014JB011304.Received.
Poveda, E., Julià, J., Schimmel, M., Perez-Garcia, N., 2018. Upper and middle crustal velocity structure of the Colombian Andes from ambient noise tomography: investigating subduction-related magmatism in the overriding plate. J. Geophys. Res. Solid Earth 123, 1459–1485. https://doi.org/10.1002/2017JB014688.
Prowatke, S., Klemme, S., 2006. Trace element partitioning between apatite and silicate melts. Geochim. Cosmochim. Acta 70, 4513–4527. https://doi.org/10.1016/j.gca.2006.06.162.
Rapp, R.P., 1995. Amphibole-out phase boundary in partially melted metabasalt, its control over liquid fraction and composition, and source permeability. J. Geophys. Res. Solid Earth 100, 15601–15610. https://doi.org/10.1029/95JB00913.

Rapp, R.P., Watson, E.B., 1995. Dehydration melting of metabasalt at 8-32 kbar: Implications for continental growth and crust-mantle recycling. J. Petrol. 36, 891–931. https://doi.org/10.1093/petrology/36.4.891.
Rapp, R.P., Shimizu, N., Norman, M.D., 2003. Growth of early continental crust by partial melting of eclogite. Nature 425, 605–609. https://doi.org/10.1038/nature02031.
Rollinson, H.R., 1993. Using Geochemical Data. https://doi.org/10.4324/9781315845548.
Rudnick, R.L., 1995. Making continental crust. Nature 378, 571–578. https://doi.org/10.1038/378571a0.
Rudnick, R.L., 2000. Rutile-bearing refractory eclogites: Missing link between continents and depleted mantle. Science 287, 278–281. https://doi.org/10.1126/science.287.5451.278.
Rudnick, R.L., Fountain, D.M., 1995. Nature and composition of the continental-crust - a lower crustal perspective. Rev. Geophys. 33, 267–309. https://doi.org/10.1029/95rg01302.
Schmidt, M.W., Poli, S., 2013. Devolatilization during subduction. Treatise on Geochemistry, 2nd ed. Elsevier Ltd https://doi.org/10.1016/B978-0-08-095975-7.00321-1.
Sen, C., Dunn, T., 1994. Dehydration melting of a basaltic composition amphibolite at 1.5 and 2.0 GPa: implications for the origin of adakites. Contrib. Mineral. Petrol. 117, 394–409. https://doi.org/10.1007/BF00307273.
Skora, S., Blundy, J.D., Brooker, R.A., Green, E.C.R., de Hoog, J.C.M., Connolly, J.A.D., 2015. Hydrous phase relations and trace element partitioning behaviour in calcareous sediments at subduction-zone conditions. J. Petrol. 56, 953–980. https://doi.org/10.1093/petrology/egv024.
Spandler, C., Pirard, C., 2013. Element recycling from subducting slabs to arc crust: a review. Lithos 170–171, 208–223. https://doi.org/10.1016/j.lithos.2013.02.016.
Straub, S.M., Gomez-Tuena, A., Stuart, F.M., Zellmer, G.F., Espinasa-Perena, R., Cai, Y., Iizuka, Y., 2011. Formation of hybrid arc andesites beneath thick continental crust. Earth Planet. Sci. Lett. 303, 337–347. https://doi.org/10.1016/j.epsl.2011.01.013.
Straub, S.M., Gómez-Tuena, A., Bindeman, I.N., Bolge, L.L., Brandl, P.A., Espinasa-Perena, R., Solari, L., Stuart, F.M., Vannucchi, P., Zellmer, G.F., 2015. Crustal recycling by subduction erosion in the central Mexican Volcanic Belt. Geochim. Cosmochim. Acta 166, 29–52. https://doi.org/10.1016/J.GCA.2015.06.001.
Syracuse, E.M., van Keken, P.E., Abers, G.A., Suetsugu, D., Bina, C., Inoue, T., Wiens, D., Jellinek, M., 2010. The global range of subduction zone thermal models. Phys. Earth Planet. Inter. 183, 73–90. https://doi.org/10.1016/j.pepi.2010.02.004.
Syracuse, E.M., Maceira, M., Prieto, G.A., Zhang, H., Ammon, C.J., 2016. Multiple plates subducting beneath Colombia, as illuminated by seismicity and velocity from the joint inversion of seismic and gravity data. Earth Planet. Sci. Lett. 444, 139–149. https://doi.org/10.1016/j.epsl.2016.03.050.
Tanaka, T., Togashi, S., Kamioka, H., Amakawa, H., Kagami, H., Hamamoto, T., Yuhara, M., Orihashi, Y., Yoneda, S., Shimizu, H., Kunimaru, T., Takahashi, K., Yanagi, T., Nakano, T., Fujimaki, H., Shinjo, R., Asahara, Y., Tanimizu, M., Dragusanu, C., 2000. JNdi-1: a neodymium isotopic reference in consistency with LaJolla neodymium. Chem. Geol. 168, 279–281. https://doi.org/10.1016/S0009-2541(00)00198-4.
Taylor, S.R., 1967. The origin and growth of continents. Tectonophysics 4, 17–34. https://doi.org/10.1016/0040-1951(67)90056-X.
Thouret, J.C., Cantagrel, J.M., Salinas, R., Murcia, A., 1990. Quaternary eruptive history of Nevado del Ruiz (Colombia). J. Volcanol. Geotherm. Res. 41, 225–251. https://doi.org/10.1016/0377-0273(90)90090-3.
Todt, W., Cliff, R.A., Hanser, A., Hofmann, A.W., 1996. Evaluation of a 202 Pb- 205 Pb Double Spike for High - Precision Lead Isotope Analysis. American Geophysical Union (AGU), pp. 429–437 https://doi.org/10.1029/GM095p0429.
Tsuno, K., Dasgupta, R., Danielson, L., Righter, K., 2012. Flux of carbonate melt from deeply subducted pelitic sediments: geophysical and geochemical implications for the source of Central American volcanic arc. Geophys. Res. Lett. 39, 1–7. https://doi.org/10.1029/2012GL052606.
van de Flierdt, T., Frank, M., Lee, D.C., Halliday, A.N., Reynolds, B.C., Hein, J.R., 2004. New constraints on the sources and behavior of neodymium and hafnium in seawater from Pacific Ocean ferromanganese crusts. Geochim. Cosmochim. Acta 68, 3827–3843. https://doi.org/10.1016/j.gca.2004.03.009.
Vatin-Pérignon, N., Goemans, P., Oliver, R.A., Briqueu, L., Thouret, J.C., Salinas, R., Murcia, A., 1988. Magmatic evolution of the Nevado del Ruiz volcano, Central Cordillera, Colombia: mineral chemistry and geochemistry. Géodynamique, ORSTOM 3, 163–194.
Vatin-Pérignon, N., Goemans, P., Oliver, R.A., Palacio, E.P., 1990. Evaluation of magmatic processes for the products of the Nevado del Ruiz Volcano, Colombia from geochemical and petrological data. J. Volcanol. Geotherm. Res. 41, 153–176. https://doi.org/10.1016/0377-0273(90)90087-V.
Vervoort, J.D., Patchett, P.J., Blichert-Toft, J., Albarède, F., 1999. Relationships between Lu-Hf and Sm-Nd isotopic systems in the global sedimentary system. Earth Planet. Sci. Lett. 168, 79–99. https://doi.org/10.1016/S0012-821X(99)00047-3.
Vervoort, J.D., Plank, T., Prytulak, J., 2011. The Hf-Nd isotopic composition of marine sediments. Geochim. Cosmochim. Acta 75, 5903–5926. https://doi.org/10.1016/j.gca.2011.07.046.
Villagómez, D., Spikings, R., Magna, T., Kammer, A., Winkler, W., Beltrán, A., 2011. Geochronology, geochemistry and tectonic evolution of the Western and Central cordilleras of Colombia. Lithos 125, 875–896. https://doi.org/10.1016/j.lithos.2011.05.003.
Villamil, T., 1999. Campanian-Miocene tectonostratigraphy, depocenter evolution and basin development of Colombia and western Venezuela. Palaeogeogr. Palaeoclimatol. Palaeoecol. 153, 239–275. https://doi.org/10.1016/S0031-0182(99)00075-9.
Weber, M.B.I., 1998. The Mercaderes-Rio Mayo Xenoliths, Colombia: Their Bearing on Mantle and Crustal Processes in the Northern Andes. Ph.D Thesis. Leicester University, UK.
Weber, M.B.I., Tarney, J., Kempton, P.D., Kent, R.W., 2002. Crustal make-up of the Northern Andes: evidence based on deep crustal xenolith suites, Mercaderes, SW Colombia. Tectonophysics 345, 49–82. https://doi.org/10.1016/S0040-1951(01)00206-2.
Woodland, A.B., Bulatov, V.K., Brey, G.P., Girnis, A.V., Höfer, H.E., Gerdes, A., 2018. Subduction factory in an ampoule: experiments on sediment–peridotite interaction under temperature gradient conditions. Geochim. Cosmochim. Acta 223, 319–349. https://doi.org/10.1016/j.gca.2017.12.012.
Workman, R.K., Hart, S.R., 2005. Major and trace element composition of the depleted MORB mantle (DMM). Earth Planet. Sci. Lett. 231, 53–72. https://doi.org/10.1016/j.epsl.2004.12.005.
Workman, R.K., Hart, S.R., Jackson, M., Regelous, M., Farley, K.A., Blusztajn, J., Kurz, M., Staudigel, H., 2004. Recycled metasomatized lithosphere as the origin of the Enriched Mantle II (EM2) end-member: evidence from the Samoan Volcanic Chain. Geochem. Geophys. Geosyst. 5, 1–44. https://doi.org/10.1029/2003GC000623.
Xiao, Y., Niu, Y., Song, S., Davidson, J., Liu, X., 2013. Elemental responses to subduction-zone metamorphism: Constraints from the North Qilian Mountain, NW China. Lithos 160–161, 55–67. https://doi.org/10.1016/j.lithos.2012.11.012.
Yarce, J., Monsalve, G., Becker, T.W., Cardona, A., Poveda, E., Alvira, D., Ordoñez-Carmona, O., 2014. Seismological observations in Northwestern South America: evidence for two subduction segments, contrasting crustal thicknesses and upper mantle flow. Tectonophysics 637, 57–67. https://doi.org/10.1016/j.tecto.2014.09.006.
Zellmer, G.F., Iizuka, Y., Miyoshi, M., Tamura, Y., Tatsumi, Y., 2012. Lower crustal H2O controls on the formation of adakitic melts. Geology 40, 487–490. https://doi.org/10.1130/G32912.1.